International Journal for Numerical and Analytical Methods in Geomechanics

WILEY

RESEARCH ARTICLE

PML-Based Family of Stretched Coordinate Systems for Wave Propagation in Poroelastic Transversely Isotropic Half-Space

Kamal Shaker | Morteza Eskandari-Ghadi | Soheil Mohammadi

School of Civil Engineering, College of Engineering, University of Tehran, Tehran, Iran

Correspondence: Morteza Eskandari-Ghadi (ghadi@ut.ac.ir)

Received: 17 March 2025 | **Revised:** 17 March 2025 | **Accepted:** 28 March 2025

Funding: The authors received no specific funding for this work.

Keywords: perfectly matched layer | poroelastic transversely isotropic | potential function stretched coordinate transformation | wave propagation

ABSTRACT

Investigating wave propagation in transversely isotropic saturated poroelastic material and introducing a family of stretched coordinate transformations to be used for defining a perfectly matched layer (PML) are the main aims of this paper. To this end, the $\mathbf{u} - p$ formulation of Biot is adopted as the governing framework of the porous media. The coupled equations of motion and transport equation are uncoupled by means of the recently proposed two scalar potential functions in cylindrical coordinate system. Two separated families of continuous stretched coordinate transformations are introduced for each of radial and axial coordinates, which allows the whole half-space to be replaced by a finite cylinder surrounded by an outer cylinder/cube with both finite height and radius. It is shown that the displacements and pore fluid pressure, determined from the analysis of the replaced cylindrical domain, is exactly collapsed on the analytical solution in the inner cylinder, while they are, based on the stretched coordinate transformation, attenuated very fast in the outer cylinder to prevent the reflection from the most exterior boundaries. The results of this study may be used in any wave propagation analysis containing either isotropic or transversely isotropic half- or full-space.

1 | Introduction

The subject of wave propagation in unbounded/semiunbounded domains has been of great interest for engineers and mathematicians. Researchers have widely used Biot's theory and its simplified formulations to investigate the interaction between structures and their supporting soil. Different shapes of both internal and surface loading foundations, including circular [1–3], rectangular [4, 5] and arbitrary shape [6, 7] foundations, and either pure elastic or porous media have been considered to analyze the dynamic responses of single/multi-layered elastic/poroelastic media. To solve the boundary value problem (BVP) of wave propagation in transversely isotropic porous media different strategies have been employed among them one can mention the potential-function method [8–12] and the cylindrical system of vector functions [13–15] for decoupling the governing partial differential equations and converting them to sets of ordinary differential equations. In the case of layered media, Zhang and Pan [14, 15] employed the dual variable and position method to establish a recursive relation for the field quantities. Chen [16] studied a saturated layered half-space subjected to the vibration of a flexible foundation by means of the Hankel transform technique. Moreover, the poroelastic media under different loads have been investigated by utilizing a discretization technique and the influence functions obtained from the stiffness matrix method [6, 17–19].

The geometry attenuation of the energy transmitted by the waves in these types of domains, denoted as radiation condition, is one of the challenging physical phenomena in the investigation of the wave propagation in unbounded/semiunbounded domains. Based on the rule of the radiation condition, no incoming wave from the remote boundary exists in unbounded/semiunbounded domains. Although deriving analytical solutions for complex BVPs is not easy, considering the radiation condition in the analytical solution is not complicated. However, many related BVPs cannot be treated analytically; thus, a numerical approach should be followed. On the other hand, satisfying the radiation condition in a numerical approach needs special attention. The subject has been studied for many years with the use of different numerical-based approaches [20–27].

One of the methods for imposing the radiation condition is to use the perfectly matched layer (PML) concept [28–32]. A PML is a finite thickness layer that quickly attenuates the energy transmitted by the wave traveling toward infinity. The amplitudes of different functions are smoothly limiting to zero along this layer in such a way that no wave reflects from the far boundary of PML. By this explanation, an unbounded/semiunbounded domain is divided into two subdomains, namely, near field and far field. The near field is defined as a subdomain, where the accuracy of different response functions is important, and the far field is the remaining part, where the accuracy of the solutions is not important at all, while the speed of attenuation of different functions at the outer boundary is important. By replacing the whole unbounded/semiunbounded domain with the union of near field and PML, a bounded domain is resulted, which is appropriate for numerical analysis of wave propagation.

The main idea to satisfy the radiation condition in a PML is to model the far field as close as possible to the near field without affecting the actual physical behavior of any interested functions in the near field. Since different functions involved in wave propagation in unbounded/semiunbounded domain are completely radiated at infinity, one may use a one-by-one continuous transformation function to map the unbounded far field approximately to a finite thickness layer, where the end of the layer is an approximate image for infinity. In this way, the values of different functions at the far boundary of the PML are approximately equal to their values at infinity (as close as possible to zero based on radiation condition). The PML may make a platform for increasing the accuracy and decreasing the cost of numerical analysis of soil-structure-interaction (SSI) as one of the applications of the theory of wave propagation in solids.

Givoli defined high-order nonreflecting boundary conditions to be used in finite element analysis of either infinite or semiinfinite domain boundary value wave propagation problems [20, 33, 34], ensuring the energy traveling to infinity would not return to the domain, as it is in real physics. However, inventing the PML concept was a revolution in the subject, which was first introduced by Berenger [30] in the context of electromagnetic wave propagation. Other researchers extended the subject to electromagnetics and electrodynamics [32, 35, 36], as well as in elastic wave propagation in Cartesian, cylindrical, and spherical coordinate systems. Basu and Chopra [28, 29] have made precise and applicable formulations for time harmonic and transient wave propagation in unbounded elastic media. They clearly explained the problem for one dimensional wave propagation and extended the procedure to the three-dimensional case. Zeng et al., combined the finite difference method with PML to study the wave propagation in poroelastic materials in the framework of $\mathbf{u}-\mathbf{u}$ formulation derived from the Biot's theory [37]. The mathematical requirement for this problem was based on the concept of wave propagation in infinite domains [38, 39]. Numerical solution for this kind of problems in the framework of general domain-based numerical methods, such as finite element method (FEM), would need inclusion of an absorbing boundary at the far field [21–23]. Recently, based on the meshless method, Shaker et al. have been used the PML to study the wave propagation in the poroelastic transversely isotropic half-space [40].

This paper presents a family of stretching functions to define the stretched coordinate system. With the use of the new family of stretching functions, the infinite domain can be modeled as a finite domain to be used in any domain-based numerical analysis such as finite element and meshless methods. To investigate various aspects of the presented family of stretched coordinate system, stress wave propagation due to an arbitrary time-harmonic finite patch surface load in a half-space containing either elastic or poroelastic transversely isotropic material in both mechanical- and transport-points of view, in which SV- and different P-waves are coupled, is considered. Thus, this study prepares a framework to deal with radiation conditions with the use of PML in these complicated materials for the first time. To this end, the Biot $\mathbf{u}-p$ formulation is accepted as the governing equations for the whole half-space. A potential function method introduced in [8] is applied to uncouple the partial differential equations as a transformation of the originally coupled equations of motion and transport in the cylindrical coordinate system. Based on the analytical solutions for the potential functions, and thus for the displacements and pore fluid pressure, two separate families of continuous stretched coordinate transformations are introduced to make PML in both radial and vertical directions.

The gradient of the attenuation of different functions is controlled with the use of some scalar parameters proposed in the stretched coordinate transformations, which are reduced to only one parameter in each direction based on both physical and mathematical justifications for the attenuation of the solutions. The analysis is first performed for an axis-symmetric case, and then is extended to the general asymmetric case. In addition, the controlling parameters that exist in the stretched coordinate transformations are first investigated in detail for an outgoing wave, and then they are checked for both outgoing and incoming waves.

It is shown that the numerical results are exactly collapsed on the analytical solutions in near field, while they are attenuated in the far field as fast as the user desire. The procedure can be easily used for any domain-based solution, either mesh-dependent or mesh-free numerical analyses. The whole procedure can be applied to any domain containing transversely isotropic material in both mechanical and transport points of view. Since isotropic material is a degeneration of transversely isotropic one, the proposed procedure is directly used for isotropic material as well. The proposed procedure may be used in any wave propagation analysis containing either isotropic or transversely isotropic half- or full-space.

The structure of the paper is in the following form: In Section 2, wave propagation due to an arbitrary time-harmonic finite surface excitation applied on a half-space containing a transversely isotropic mechanical and transport material is considered. Based on the terms appearing in the response functions, a family of transferring/stretching function is introduced in Section 3. Some degenerations of the general problem are expressed in Section 4. In addition, in Section 5, the results of this study are compared with the analytical solutions and more simplified forms are presented for the stretching functions by reducing their parameters. Eventually, the conclusion is drowned in Section 6.

2 | Governing Equation

A saturated poroelastic material with transversely isotropic mechanical and transport characteristics is considered, in such a way that the material axes of symmetry for both deformation and flow of fluid are parallel. The governing equations of motion and Darci's law in the framework of $\mathbf{u}-p$ formulation, as a simplified version of Biot's formulation may be written in the form of [41, 42]

$$\begin{aligned} &\nabla\cdot\boldsymbol{\sigma}+\rho\mathbf{b}=\rho\ddot{\mathbf{u}}\\ &\dot{\mathbf{w}}=\frac{\mathbf{k}}{\eta}(-\nabla p+\rho^f\mathbf{b}-\rho^f\ddot{\mathbf{u}}), \end{aligned}\tag{1}$$

where the pore fluid acceleration with respect to the solid is neglected. $\boldsymbol{\sigma}$ is the total Cauchy stress tensor, $\mathbf{u}$ is the displacement vector of solid skeleton, $\mathbf{w}$ is the relative displacement vector of fluid with respect to the solid skeleton, p is the pore fluid pressure, and $\mathbf{b}$ is the body force vector. ρ^f, ρ^s, and $\rho=(1-n)\rho^s+n\rho^f$ are the fluid, solid, and mixture mass densities, respectively, with n being the porosity. In addition, $\mathbf{k}$ is the intrinsic permeability tensor and η is the dynamic viscosity of fluid. It should be mentioned that $\mathbf{k}$ is a diagonal matrix, with two independent eigenvalues for a transversely isotropic material. It worth mentioning that the anisotropy behavior for mechanical and transport properties are independent, meaning that each of the mechanical and transport properties can be either isotropic or transversely isotropic.

The continuity condition for the fluid in a volume control may be expressed in the form of [43]

$$\frac{\partial\zeta}{\partial t}+\nabla\cdot\dot{\mathbf{w}}=0\tag{2}$$

where ζ represents the change of fluid content in the control volume. In addition, the constitutive law, in the form of stress-displacement-pore pressure relationships (as it is in the Biot's $\mathbf{u}-p$ formulation), in a cylindrical coordinate system attached at the free surface of the half-space with a depth-wise z-axis (as seen in Figure 1 (Left)) is written as [43]

$$\begin{aligned} &\sigma_{rr}=C_{11}\frac{\partial u_r}{\partial r}+C_{12}\left(\frac{u_r}{r}+\frac{1}{r}\frac{\partial u_\theta}{\partial\theta}\right)+C_{13}\frac{\partial u_z}{\partial z}-\alpha_1 p\\ &\sigma_{\theta\theta}=C_{12}\frac{\partial u_r}{\partial r}+C_{11}\left(\frac{u_r}{r}+\frac{1}{r}\frac{\partial u_\theta}{\partial\theta}\right)+C_{13}\frac{\partial u_z}{\partial z}-\alpha_1 p\\ &\sigma_{zz}=C_{13}\frac{\partial u_r}{\partial r}+C_{13}\left(\frac{u_r}{r}+\frac{1}{r}\frac{\partial u_\theta}{\partial\theta}\right)+C_{33}\frac{\partial u_z}{\partial z}-\alpha_3 p\\ &\sigma_{rz}=C_{44}\left(\frac{\partial u_r}{\partial z}+\frac{\partial u_z}{\partial r}\right)\\ &\sigma_{\theta z}=C_{44}\left(\frac{\partial u_\theta}{\partial z}+\frac{1}{r}\frac{\partial u_z}{\partial\theta}\right)\\ &\sigma_{r\theta}=C_{66}\left(\frac{1}{r}\frac{\partial u_r}{\partial\theta}+\frac{\partial u_\theta}{\partial r}-\frac{u_\theta}{r}\right)\\ &p=-\alpha_1 M\left(\frac{\partial u_r}{\partial r}+\frac{u_r}{r}+\frac{1}{r}\frac{\partial u_\theta}{\partial\theta}\right)-\alpha_3 M\frac{\partial u_z}{\partial z}+M\zeta \end{aligned}\tag{3}$$

where C_{ij} $(i,j=1-6)$ is the drained elasticity coefficient tensor of material in Voigt notation and M is the Biot's modulus. In addition

$$\alpha_1=1-\frac{C_{11}+C_{12}+C_{13}}{3K_s},\ \alpha_3=1-\frac{2C_{13}+C_{33}}{3K_s}\tag{4}$$

in which K_s is the bulk moduli of solid matrix. Rewriting Equation (1) by substituting the stresses in terms of the displacements and pore fluid pressure, as given in Equation (3), results in the equations of motion and Darci's law in terms of displacements and pore fluid pressure as

$$\begin{aligned} &(1+\beta_1)\left(\frac{\partial^2 u_r}{\partial r^2}+\frac{1}{r}\frac{\partial u_r}{\partial r}-\frac{u_r}{r^2}\right)+\beta_2\frac{\partial^2 u_r}{\partial z^2}+\frac{1}{r^2}\frac{\partial^2 u_r}{\partial\theta^2}\\ &+\beta_1\left(\frac{1}{r}\frac{\partial^2 u_\theta}{\partial r\partial\theta}+\frac{1}{r^2}\frac{\partial u_\theta}{\partial\theta}\right)-2(1+\beta_1)\frac{1}{r^2}\frac{\partial u_\theta}{\partial\theta}+\beta_3\frac{\partial^2 u_z}{\partial r\partial z}\\ &-\bar{\alpha}_1\frac{\partial p}{\partial r}+\bar{\rho}b_r=\bar{\rho}\frac{\partial^2 u_r}{\partial t^2}\\ &\beta_1\left(\frac{1}{r}\frac{\partial^2 u_r}{\partial r\partial\theta}-\frac{1}{r^2}\frac{\partial u_r}{\partial\theta}\right)\\ &+2(1+\beta_1)\frac{1}{r^2}\frac{\partial u_r}{\partial\theta}+\left(\frac{\partial^2 u_\theta}{\partial r^2}+\frac{1}{r}\frac{\partial u_\theta}{\partial r}-\frac{u_\theta}{r^2}\right)\\ &+(1+\beta_1)\frac{1}{r^2}\frac{\partial^2 u_\theta}{\partial\theta^2}+\beta_2\frac{\partial^2 u_\theta}{\partial z^2}+\beta_3\frac{1}{r}\frac{\partial^2 u_z}{\partial\theta\partial z}\\ &-\bar{\alpha}_1\frac{1}{r}\frac{\partial p}{\partial\theta}+\bar{\rho}b_\theta=\bar{\rho}\frac{\partial^2 u_\theta}{\partial t^2}\\ &\beta_3\left(\frac{\partial^2 u_r}{\partial r\partial z}+\frac{1}{r}\frac{\partial u_r}{\partial z}+\frac{1}{r}\frac{\partial^2 u_\theta}{\partial\theta\partial z}\right)+\beta_2\left(\frac{\partial^2 u_z}{\partial r^2}+\frac{1}{r}\frac{\partial u_z}{\partial r}+\frac{1}{r^2}\frac{\partial^2 u_z}{\partial\theta^2}\right)\\ &+\beta_4\frac{\partial^2 u_z}{\partial z^2}-\bar{\alpha}_3\frac{\partial p}{\partial z}+\bar{\rho}b_z=\bar{\rho}\frac{\partial^2 u_z}{\partial t^2}\\ &\left(\rho_f\bar{k}_1\frac{\partial^2}{\partial t^2}-\bar{\alpha}_1\eta\frac{\partial}{\partial t}\right)\left(\frac{u_r}{r}+\frac{\partial u_r}{\partial r}+\frac{1}{r}\frac{\partial u_\theta}{\partial\theta}\right)\\ &+(\rho_f\bar{k}_3\frac{\partial^2}{\partial t^2}-\bar{\alpha}_3\eta\frac{\partial}{\partial t})\frac{\partial u_z}{\partial z}\\ &+\bar{k}_1\left(\frac{\partial^2 p}{\partial r^2}+\frac{1}{r}\frac{\partial p}{\partial r}+\frac{1}{r^2}\frac{\partial^2 p}{\partial\theta^2}\right)+\bar{k}_3\frac{\partial^2 p}{\partial z^2}-\beta_5\frac{\partial p}{\partial t}\\ &-\bar{k}_1\rho_f\left(\frac{b_r}{r}+\frac{\partial b_r}{\partial r}+\frac{1}{r}\frac{\partial b_\theta}{\partial\theta}\right)-\bar{k}_3\rho_f\frac{\partial b_z}{\partial z}=0 \end{aligned}\tag{5}$$

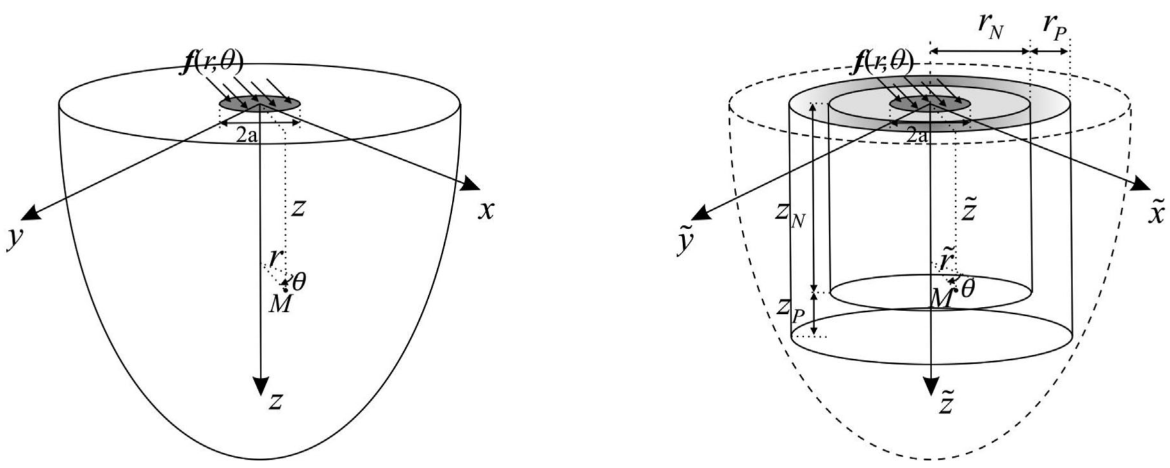

FIGURE 1 | In PML approach, the original half-space (left) is truncated and the stretched coordinate system for the truncated domain (right) is defined in such a way that the response functions in the near field are equal to the original domain and they are attenuated in PML. (left) The original half-space undergoing some arbitrary traction on a finite part at the surface of the domain, (right) the truncated domain consists of the near field (the cylinder with radius r_N and height z_N) and PML (the hollow cylinder surrounding the near field which is specified by r_P and z_P) in the stretched coordinate system $o\tilde{x}\tilde{y}\tilde{z}$. PML, perfectly matched layer.

where

$$\beta_1 = \frac{C_{12}+C_{66}}{C_{66}}, \beta_2 = \frac{C_{44}}{C_{66}}, \beta_3 = \frac{C_{13}+C_{44}}{C_{66}}, \beta_4 = \frac{C_{33}}{C_{66}},$$
$$\beta_5 = \frac{\eta}{MC_{66}}, \bar{\rho} = \frac{\rho}{C_{66}},$$
$$\bar{k}_l = \frac{k_l}{C_{66}}, \bar{\alpha}_l = \frac{\alpha_l}{C_{66}}, \qquad l = 1,3 \tag{6}$$

Equations (5) are known as $\mathbf{u} - p$ formulation for transversely isotropic saturated poroelastic materials [8]. These equations are solved for a half-space containing transversely isotropic saturated poroelastic materials, under some time-harmonic surface traction applied on a finite patch. Since the relative fluid acceleration with respect to solid is neglected, the governing equations are valid to frequencies limited by [44]

$$f_t = \frac{\pi\nu}{4d^2} \tag{7}$$

in which d is the order of pore diameter and ν is the kinematic viscosity of fluid [45]. The restriction given in Equation (7) implies that the larger the pore size and the smaller the viscosity results in the smaller the upper bound of the valid frequency of excitation.

3 | PML Formulations

The half-space under consideration is divided into two separated parts, namely near field and far field (see Figure 1). The near field is defined as a bounded region subjected to the external excitation, where the accuracy of the displacements, stresses and pore fluid pressure due to wave propagation are important. On the other hand, the far field is defined as an unbounded domain surrounding the near field and extended to infinity, where only outgoing waves are propagated in. The far field is replaced with a finite region, so that the whole half-space is modeled with a bounded domain. In this way, one may make a framework for the BVP to be solved based on an adopted domain-related numerical procedure, such as the FEM. The accuracy of the solutions in the far field is not important, and one only needs to be aware of the continuity conditions from the near field to the far field, and zero amplitude reflected wave from the far boundary of the finite region replaced for the far field.

The PML formulation is one approach which uses a bounded near field surrounded by a finite-thickness layer in replace of the unbounded remaining domain to reduce the computational cost in domain-based numerical methods. Outgoing waves are absorbed, almost perfectly, through this layer with no reflection from its boundary. So, the near field solution remains as accurate as the analytical method. On the other hand, while the solution in far field is not correct, it does not affect the accuracy of the solution in the near field. In this way, with the use of a frequency-independent complex stretching function, one may produce the standard PML formulation. The frequency-independent complex coordinate stretching function is defined as [46]:

$$\tilde{r} := \int_0^r \lambda_r(s)ds,\ \tilde{\theta} := \int_0^\theta \lambda_z(s)ds,\ \tilde{z} := \int_0^z \lambda_z(s)ds \tag{8}$$

where the so-called complex-valued coordinate stretching functions $\lambda_r, \lambda_\theta$, and λ_z are defined on the far field, which are nowhere zero and continuous everywhere. Accordingly, the stretched coordinate system $(\tilde{r}, \tilde{\theta}, \tilde{z})$ is used to rewrite the governing equations.

3.1 | Governing Equations in the Stretched Coordinate System

By virtue of potential functions, one may uncouple the coupled equations of motion and the transport equation to derive some equivalent separated partial differential equations for the potential functions. The proposed stretched coordinate system is applied on the decoupled equations governing the potential functions as transformations of the motion and transport equations.

Adopting the two recently introduced scalar potential functions denoted as F and χ (see [8]) the displacements and the pore fluid pressure are written in terms of these two scalar potential functions in the stretched coordinate system as

$$
\begin{aligned}
u_r &= -\bar{k}_1\beta_3 \frac{\partial^2}{\partial\tilde{r}\partial\tilde{z}}\left(\Box_p{}^2 + \frac{\bar{\alpha}_1\bar{k}_3}{\beta_3\bar{k}_1}\rho_f\frac{\partial^2}{\partial t^2} - \eta\frac{\bar{\alpha}_1\bar{\alpha}_3}{\beta_3\bar{k}_1}\frac{\partial}{\partial t}\right)F - \frac{1}{\tilde{r}}\frac{\partial\chi}{\partial\tilde{\theta}}\\
u_\theta &= -\bar{k}_1\beta_3\frac{1}{\tilde{r}}\frac{\partial^2}{\partial\tilde{\theta}\partial\tilde{z}}\left(\Box_p^2 + \frac{\bar{\alpha}_1\bar{k}_3}{\beta_3\bar{k}_1}\rho_f\frac{\partial^2}{\partial t^2} - \eta\frac{\bar{\alpha}_1\bar{\alpha}_3}{\beta_3\bar{k}_1}\frac{\partial}{\partial t}\right)F + \frac{\partial\chi}{\partial\tilde{\theta}}\\
u_z &= \bar{k}_1\left[\left(\Box_0^2 + \beta_1\nabla^2_{\tilde{r}\tilde{\theta}}\right)\Box_p^2 + \bar{\alpha}_1\nabla^2_{\tilde{r}\tilde{\theta}}\left(\rho_f\frac{\partial^2}{\partial t^2} - \eta\frac{\bar{\alpha}_1}{\bar{k}_1}\frac{\partial}{\partial t}\right)\right]F\\
p &= -\frac{\partial^2}{\partial t\partial\tilde{z}}\left[-\eta\bar{\alpha}_3\left(\Box_0^2 + \left(\beta_1 - \beta_3\frac{\bar{\alpha}_1}{\bar{\alpha}_3}\right)\nabla^2_{\tilde{r}\tilde{\theta}}\right)\right.\\
&\quad\left. + \bar{k}_3\rho_f\frac{\partial}{\partial t}\left(\Box_0^2 + \left(\beta_1 - \beta_3\frac{\bar{k}_1}{\bar{k}_3}\right)\nabla^2_{\tilde{r}\tilde{\theta}}\right)\right]F
\end{aligned}
\tag{9}
$$

where

$$
\begin{aligned}
\nabla^2_{\tilde{r}\tilde{\theta}} &= \frac{\partial^2}{\partial\tilde{r}^2} + \frac{1}{\tilde{r}}\frac{\partial}{\partial\tilde{r}} + \frac{1}{\tilde{r}^2}\frac{\partial^2}{\partial\tilde{\theta}^2}\\
\Box_0^2 &= \nabla^2_{\tilde{r}\tilde{\theta}} + \beta_2\frac{\partial^2}{\partial\tilde{z}^2} - \bar{\rho}\frac{\partial^2}{\partial t^2}\\
\Box_p^2 &= \nabla^2_{\tilde{r}\tilde{\theta}} + \frac{1}{s_k^2}\frac{\partial^2}{\partial\tilde{z}^2} - \beta_k\frac{\partial}{\partial t}\\
\frac{1}{s_k^2} &= \frac{\bar{k}_3}{\bar{k}_1}, \beta_k = \frac{\beta_5}{\bar{k}_1} = \frac{\eta}{Mk_1}
\end{aligned}
\tag{10}
$$

Substituting Equation (9) into Equation (5) results in the following PDEs for the potential functions F and χ in terms of the stretched coordinate system:

$$
\begin{aligned}
&\beta_2\left[\bar{k}_1(1+\beta_1)\Box_p^2\left(\Box_1^2\Box_2^2 - \bar{\rho}\delta_3\frac{\partial^2}{\partial t^2}\frac{\partial^2}{\partial\tilde{z}^2}\right)\right.\\
&+ \bar{\alpha}_1\bar{k}_1\rho_f\frac{\partial^2}{\partial t^2}\left(\Box_{s1}^2\Box_3^2 + \delta_1\nabla^2_{\tilde{r}\tilde{\theta}}\frac{\partial^2}{\partial\tilde{z}^2}\right)\\
&\left. - \eta\bar{\alpha}_1^2\frac{\partial}{\partial t}\left(\Box_{s2}^2\Box_3^2 + \delta_2\nabla^2_{\tilde{r}\tilde{\theta}}\frac{\partial^2}{\partial\tilde{z}^2}\right)\right]F = 0\\
&\Box_0^2\chi = 0
\end{aligned}
\tag{11}
$$

where

$$
\begin{aligned}
\Box_1^2 &= \nabla^2_{\tilde{r}\tilde{\theta}} + \frac{1}{s_1^2}\frac{\partial^2}{\partial\tilde{z}^2} - \frac{\bar{\rho}}{1+\beta_1}\frac{\partial^2}{\partial t^2}\\
\Box_2^2 &= \nabla^2_{\tilde{r}\tilde{\theta}} + \frac{1}{s_2^2}\frac{\partial^2}{\partial\tilde{z}^2} - \frac{\bar{\rho}}{\beta_2}\frac{\partial^2}{\partial t^2}\\
\Box_3^2 &= \nabla^2_{\tilde{r}\tilde{\theta}} + \frac{\partial^2}{\partial\tilde{z}^2} - \frac{\bar{\rho}}{\beta_2}\frac{\partial^2}{\partial t^2}\\
\Box_{s1}^2 &= \nabla^2_{\tilde{r}\tilde{\theta}} + \frac{\bar{\alpha}_3}{\bar{\alpha}_1 s_k^2}\frac{\partial^2}{\partial\tilde{z}^2}\\
\Box_{s2}^2 &= \nabla^2_{\tilde{r}\tilde{\theta}} + \frac{\bar{\alpha}_3^2}{\bar{\alpha}_1^2}\frac{\partial^2}{\partial\tilde{z}^2}
\end{aligned}
$$

$$
\begin{aligned}
\delta_1 &= -\frac{1}{\bar{\alpha}_1\bar{k}_1\beta_2}[\bar{\alpha}_1\bar{k}_1(\beta_2-\beta_4)\\
&\quad + (\bar{\alpha}_1\bar{k}_3 + \bar{\alpha}_3\bar{k}_1)\beta_3 + \bar{\alpha}_3\bar{k}_3(\beta_2 - 1 - \beta_1)]\\
\delta_2 &= \frac{1}{\bar{\alpha}_1^2\beta_2}[\bar{\alpha}_3^2(1+\beta_1-\beta_2) + \bar{\alpha}_1^2(\beta_4-\beta_2) - 2\bar{\alpha}_1\bar{\alpha}_3\beta_3]\\
\delta_3 &= \frac{1}{1+\beta_1}\left(1 - \frac{1}{s_2^2}\right) + \frac{1}{\beta_2}\left(\frac{\beta_4}{1+\beta_1} - \frac{1}{s_1^2}\right)\\
\frac{1}{s_1^2} + \frac{1}{s_2^2} &= \frac{\beta_2^2 - \beta_3^2 + \beta_4(1+\beta_1)}{\beta_2(1+\beta_1)}, \frac{1}{s_1^2 s_2^2} = \frac{\beta_4}{1+\beta_1}.
\end{aligned}
\tag{12}
$$

Substituting the resulted F and χ from PDEs 11 in Equations (9), the displacements and the pore fluid pressure are obtained [8].

3.2 | Complete Solution to PML Problem

The free-surface of the half-space is assumed to be completely permeable; meaning that the fluid pore pressure is zero everywhere on the plane $\tilde{z} = 0$. Considering an arbitrarily distributed and arbitrarily oriented time-harmonic patch load, π_0, located at the free surface of the half-space, the boundary condition can be written as follows:

$$
\begin{aligned}
&\sigma_{\tilde{r}\tilde{z}}(\tilde{r},\tilde{\theta},0,t) = -\bar{P}(\tilde{r},\tilde{\theta})\exp(i\omega t),\\
&\sigma_{\tilde{z}\tilde{\theta}}(\tilde{r},\tilde{\theta},0,t) = -\bar{Q}(\tilde{r},\tilde{\theta})\exp(i\omega t),\\
&\sigma_{\tilde{z}\tilde{z}}(\tilde{r},\tilde{\theta},0,t) = -\bar{R}(\tilde{r},\tilde{\theta})\exp(i\omega t), \qquad (\tilde{r},\tilde{\theta}) \in \pi_0\\
&\sigma_{\tilde{r}\tilde{z}} = \sigma_{\tilde{z}\tilde{\theta}} = \sigma_{\tilde{z}\tilde{z}} = 0, \qquad (\tilde{r},\tilde{\theta}) \notin \pi_0\\
&p(\tilde{r},\tilde{\theta},0,t) = 0, \qquad \forall(\tilde{r},\tilde{\theta})
\end{aligned}
\tag{13}
$$

where the components of the patch load in $\tilde{r}$-, $\tilde{\theta}$-, and $\tilde{z}$-directions are expressed as $\bar{P}(\tilde{r},\tilde{\theta})$, $\bar{Q}(\tilde{r},\tilde{\theta})$, and $\bar{R}(\tilde{r},\tilde{\theta})$, respectively. The regularity condition at the far field should be satisfied

$$
\lim_{\sqrt{\tilde{r}^2+\tilde{z}^2}\to\infty}(u_{\tilde{r}}, u_{\tilde{\theta}}, u_{\tilde{z}}, p) = 0 \tag{14}
$$

As mentioned earlier, the unbounded domain is modeled by a near field surrounded by a PML. As seen in Figure 1, the near field is considered as a finite cylinder of radius r_N and depth z_N. The rest of the half-space is replaced by a cylindrical shell with thicknesses r_P and height z_P along $\tilde{r}$- and $\tilde{z}$- directions, respectively. To completely define the problem, one should consider proper boundary conditions on the far boundaries of PML. Here, all displacements and the flux at the far boundary of PML, i.e., $\Gamma_p = \{(r,\theta,z)|(z = z_N + z_P = z_T) \cup (r = r_N + r_P = r_T)\}$, are considered to be zero. It should be mentioned that these boundary conditions do not affect the response functions in the near field duo to zero amplitude of responses on Γ_p. So, in addition to the boundary conditions 13, the boundary conditions for this problem at the truncated surface are as follows:

$$u_r(r,\theta,z,t) = u_\theta(r,\theta,z,t) = u_z(r,\theta,z,t) = 0, \qquad (r,\theta,z) \text{ on } \Gamma_P$$
$$p(r_T,\theta,z,t) = 0, \qquad \forall(\theta,z)$$
$$q_z(r,\theta,z_T,t) = -\frac{1}{\mu}\bar{k}_3\frac{\partial p}{\partial z} - \rho_f\frac{\partial^2 u_z}{\partial t^2} = 0, \qquad \forall(r,\theta) \tag{15}$$

When the excitation is time-harmonic with the circular frequency of ω, the responses will be time-harmonic with the same circular frequency [41]. In addition, one can write these functions in the Fourier form in terms of circumferential coordinate $\tilde{\theta}$. If the domain is finite along the r-direction, one can apply the finite Hankel integral transform. As we expect the amplitude of functions attenuated along PML, and the far boundary of PML plays the role of infinity, thus the infinite Hankel integral transform can be applied. So, after applying the Hankel integral transform of order m in terms of the radial coordinate $\tilde{r}$ on the mth component of the Fourier series, one reaches to the following relationship for the functions $\mathbf{u}$, p, $\boldsymbol{\sigma}$, F, and χ:

$$[\mathbf{u}, p, \boldsymbol{\sigma}, F, \chi](\tilde{r},\tilde{\theta},\tilde{z},t)$$
$$= \exp(i\omega t)\sum_{m=-\infty}^{+\infty}\exp(im\tilde{\theta})$$
$$\times \int_0^\infty \xi\,[\hat{\bar{\mathbf{u}}}^m_m, \hat{\bar{p}}^m_m, \hat{\bar{\boldsymbol{\sigma}}}^m_m, \hat{\bar{F}}^m_m, \hat{\bar{\chi}}^m_m](\xi,\tilde{z})J(\tilde{r}\xi)d\xi \tag{16}$$

In Equation (16), $\bar{\bullet}_m$ denotes the mth component of the Fourier series, and $\hat{\bar{\bullet}}^m_m$ is the Hankel integral transform of order m after applying the Fourier transform. In addition, with the use of the boundary conditions 13, the relationships among the stress components and the surface tractions in transformed domain can be written in the following form:

$$-\hat{\bar{P}}^{m+1}_m - i\hat{\bar{Q}}^{m+1}_m = \hat{\bar{\sigma}}^{m+1}_{zrm} + i\hat{\bar{\sigma}}^{m+1}_{z\theta m},$$
$$-\hat{\bar{P}}^{m-1}_m + i\hat{\bar{Q}}^{m-1}_m = \hat{\bar{\sigma}}^{m-1}_{zrm} - i\hat{\bar{\sigma}}^{m-1}_{z\theta m},$$
$$-\hat{\bar{R}}^m_m = \hat{\bar{\sigma}}^m_{zzm}, \qquad -\hat{\bar{p}}^m_m = 0, \qquad \text{on } z = 0 \tag{17}$$

and

$$\widehat{\bar{u}}^{m+1}_{rm} + i\widehat{\bar{u}}^{m+1}_{\theta m} = 0, \widehat{\bar{u}}^{m-1}_{rm} - i\widehat{\bar{u}}^{m-1}_{\theta m} = 0, \widehat{\bar{u}}^m_{zm} = 0,$$
$$-\widehat{\bar{q}}^m_{zm} = 0, \quad \text{on} \quad \Gamma_P \tag{18}$$

In addition to relations 17 and 18 where the displacements, stresses, and pore pressure are given in terms of the potential functions $\hat{\bar{F}}^m_m(\xi,\tilde{z})$ and $\hat{\bar{\chi}}^m_m(\xi,\tilde{z})$, the flux in the Hankel–Fourier transformed space can be written as

$$\hat{\bar{q}}^m_{zm} = -\frac{1}{\mu}\bar{k}_3\frac{d\hat{\bar{p}}^m_m}{d\tilde{z}} + \rho_f\omega^2\hat{\bar{u}}^m_{zm} \tag{19}$$

To solve the BVP in the Fourier–Hankel domain, Equation (9) and the relation between stresses and potential functions are rewritten in terms of $\hat{\bar{F}}^m_m(\xi,\tilde{z})$ and $\hat{\bar{\chi}}^m_m(\xi,\tilde{z})$. After some algebraic manipulations it leads to the following relationships in the Hankel–Fourier transformed space:

$$\bar{u}^{m+1}_{\tilde{r}m} + i\bar{u}^{m+1}_{\tilde{\theta}m} = \bar{k}_1\beta_3\xi\frac{d}{d\tilde{z}}\left(\tilde{\bar{\Box}}^2_{pm} - \frac{\bar{\alpha}_1\bar{k}_3}{\beta_3\bar{k}_1}\rho_f\omega^2 - \eta\frac{\bar{\alpha}_1\bar{\alpha}_3}{\bar{k}_1\beta_3}i\omega\right)\bar{F}^m_m - i\xi\bar{\chi}^m_m$$
$$\bar{u}^{m-1}_{\tilde{r}m} - i\bar{u}^{m-1}_{\tilde{\theta}m} = -\bar{k}_1\beta_3\xi\frac{d}{d\tilde{z}}\left(\tilde{\bar{\Box}}^2_{pm} - \frac{\bar{\alpha}_1\bar{k}_3}{\beta_3\bar{k}_1}\rho_f\omega^2 - \eta\frac{\bar{\alpha}_1\bar{\alpha}_3}{\bar{k}_1\beta_3}i\omega\right)\bar{F}^m_m - i\xi\bar{\chi}^m_m$$
$$\bar{u}^m_{\tilde{z}m} = \bar{k}_1\left[(\tilde{\bar{\Box}}^2_{0m} - \beta_1\xi^2)\,\tilde{\bar{\Box}}^2_{pm} + \bar{\alpha}_1\xi^2\left(\rho_f\omega^2 + \eta\frac{\bar{\alpha}_1}{\bar{k}_1}i\omega\right)\right]\bar{F}^m_m$$
$$\bar{p}^m_m = i\omega\frac{d}{d\tilde{z}}\left[\eta\bar{\alpha}_3\left(\tilde{\bar{\Box}}^2_{0m} - \left(\beta_1 - \beta_3\frac{\bar{\alpha}_1}{\bar{\alpha}_3}\right)\xi^2\right)\right.$$
$$\left. -\bar{k}_3\rho_f i\omega\left(\tilde{\bar{\Box}}^2_{0m} - \left(\beta_1 - \beta_3\frac{\bar{k}_1}{\bar{k}_3}\right)\xi^2\right)\right]\bar{F}^m_m$$
$$\bar{\sigma}^m_{\tilde{z}\tilde{z}m} = C_{1133}\left(\bar{k}_1\beta_3\xi^2\frac{d}{d\tilde{z}}\tilde{\bar{\Box}}^2_{am}\bar{F}^m_m\right) + C_{3333}\left(\bar{k}_1\frac{d}{d\tilde{z}}\tilde{\bar{\Box}}^2_{cm}\bar{F}^m_m\right)$$
$$\bar{\sigma}^{m+1}_{\tilde{z}\tilde{r}m} + i\bar{\sigma}^{m+1}_{\tilde{z}\tilde{\theta}m} = -C_{1313}\xi\left[\bar{k}_1\left(\tilde{\bar{\Box}}^2_{cm} - \beta_3\frac{d^2}{d\tilde{z}^2}\tilde{\bar{\Box}}^2_{am}\right)\bar{F}^m_m + i\frac{d}{d\tilde{z}}\bar{\chi}^m_m\right]$$
$$\bar{\sigma}^{m-1}_{\tilde{z}\tilde{r}m} - i\bar{\sigma}^{m-1}_{\tilde{z}\tilde{\theta}m} = C_{1313}\xi\left[\bar{k}_1\left(\tilde{\bar{\Box}}^2_{cm} - \beta_3\frac{d^2}{d\tilde{z}^2}\tilde{\bar{\Box}}^2_{am}\right)\bar{F}^m_m - i\frac{d}{d\tilde{z}}\bar{\chi}^m_m\right] \tag{20}$$

where

$$\tilde{\bar{\Box}}^2_{0m} = \beta_2\frac{d^2}{d\tilde{z}^2} - \xi^2 + \bar{\rho}\omega^2,$$
$$\tilde{\bar{\Box}}^2_{pm} = \frac{1}{s_k^2}\frac{d^2}{d\tilde{z}^2} - \xi^2 - i\omega\beta_k, \; \tilde{\bar{\Box}}^2_{1m} = \frac{1}{s_1^2}\frac{d^2}{d\tilde{z}^2} - \xi^2 + \frac{\bar{\rho}\omega^2}{1+\beta_1},$$
$$\tilde{\bar{\Box}}^2_{2m} = \frac{1}{s_2^2}\frac{d^2}{d\tilde{z}^2} - \xi^2 + \frac{\bar{\rho}\omega^2}{\beta_2}, \; \bar{\Box}^2_{3m} = \frac{d^2}{d\tilde{z}^2} - \xi^2 + \frac{\bar{\rho}\omega^2}{\beta_2},$$
$$\tilde{\Box}^2_{s1m} = \frac{\bar{\alpha}_3}{\bar{\alpha}_1 s_k^2}\frac{d^2}{d\tilde{z}^2} - \xi^2, \; \tilde{\Box}^2_{s2m} = \frac{\bar{\alpha}_3^2}{\bar{\alpha}_1^2}\frac{d^2}{d\tilde{z}^2} - \xi^2, \tag{21}$$

In this way, the following ordinary differential equations derived from Equation (11) should be solved for determining $\hat{\bar{F}}^m_m(\xi,\tilde{z})$ and $\hat{\bar{\chi}}^m_m(\xi,\tilde{z})$:

$$\left(\frac{d^6}{d\tilde{z}^6} + I_3(\xi)\frac{d^4}{d\tilde{z}^4} + I_2(\xi)\frac{d^2}{d\tilde{z}^2} + I_1(\xi)\right)\hat{\bar{F}}^m_m(\xi,\tilde{z}) = 0,$$
$$\left(\frac{d^2}{d\tilde{z}^2} + I_4(\xi)\right)\hat{\bar{\chi}}^m_m(\xi,\tilde{z}) = 0, \tag{22}$$

in which the coefficients I_i $(i = 1-4)$ are as follows:

$$I_4(\xi) = \frac{1}{\beta_2}\left(\bar{\rho}\omega^2 - \xi^2\right),$$
$$\phi_1 I_3(\xi) = -\phi_2\xi^2 + \phi_3$$
$$-i\omega\left(\frac{\beta_k}{s_1^2 s_2^2} + \frac{\eta\bar{\alpha}_3^2}{\bar{k}_1(1+\beta_1)}\right) - \frac{\bar{\alpha}_3\rho_f\omega^2}{s_k^2(1+\beta_1)},$$
$$\phi_1 I_2(\xi) = \phi_4\xi^4 + \phi_5\xi^2 + \phi_6$$
$$+\frac{i\omega\eta}{\bar{k}_1(1+\beta_1)}\left[\bar{\alpha}_1^2(1+\delta_2)\xi^2 + \bar{\alpha}_3^2\left(\xi^2 - \frac{\bar{\rho}\omega^2}{\beta_2}\right)\right]$$
$$+\frac{\rho_f\omega^2}{\bar{k}_1(1+\beta_1)}\left[\bar{k}_1\bar{\alpha}_1(1+\delta_1)\xi^2 + \bar{k}_3\bar{\alpha}_3\left(\xi^2 - \frac{\bar{\rho}\omega^2}{\beta_2}\right)\right],$$

$$\begin{aligned}\phi_1 I_1(\xi) &= -\xi^6 + \phi_7\xi^4 + \phi_8\xi^2 + \phi_9 \\ &- \frac{\bar{\alpha}_1\xi^2}{(1+\beta_1)}\left(\xi^2 - \frac{\bar{\rho}\omega^2}{\beta_2}\right)\left(i\omega\eta\frac{\bar{\alpha}_1}{\bar{k}_1} + \rho_f\omega^2\right),\end{aligned} \tag{23}$$

and ϕ_i $(i = 1-9)$ are defined as

$$\begin{aligned}
\phi_1 &= \frac{1}{(s_1 s_2 s_k)^2},\ \phi_2 = \frac{1}{s_1^2 s_2^2} + \frac{1}{s_k^2}\left(\frac{1}{s_1^2} + \frac{1}{s_2^2}\right), \\
\phi_3 &= \frac{\bar{\rho}\omega^2}{s_k^2}\left(\frac{\beta_2+\beta_4}{\beta_2(1+\beta_1)}\right),\ \phi_4 = \frac{1}{s_1^2} + \frac{1}{s_2^2} + \frac{1}{s_k^2}, \\
\phi_5 &= -\bar{\rho}\omega^2\left[\frac{1}{s_k^2}\left(\frac{1}{(1+\beta_1)} + \frac{1}{\beta_2}\right) + \frac{\beta_2+\beta_4}{\beta_2(1+\beta_1)}\right] \\
&\quad + i\omega\beta_k\left(\frac{1}{s_1^2} + \frac{1}{s_2^2}\right), \\
\phi_6 &= -i\omega^3\bar{\rho}\beta_k\left(\frac{\beta_2+\beta_4}{\beta_2(1+\beta_1)}\right) + \frac{\bar{\rho}^2\omega^4}{s_k^2\beta_2(1+\beta_1)}, \\
\phi_7 &= \bar{\rho}\omega^2\left(\frac{1}{1+\beta_1} + \frac{1}{\beta_2}\right) - i\omega\beta_k, \\
\phi_8 &= \frac{\bar{\rho}\omega^2}{\beta_2(1+\beta_1)}[i\omega\beta_k(1+\beta_1+\beta_2) - \bar{\rho}\omega^2],\ \phi_9 = -\frac{i\omega^5\beta_k\bar{\rho}^2}{\beta_2(1+\beta_1)},
\end{aligned} \tag{24}$$

The characteristic equations of Equations (22) are given as

$$\begin{aligned}
&\lambda_i^6 + I_3(\xi)\lambda_i^4 + I_2(\xi)\lambda_i^2 + I_1(\xi) = 0, \qquad i = 1,2,3 \\
&\lambda_4^2 + I_4(\xi) = 0,
\end{aligned} \tag{25}$$

which lead to the following solution for Equations (22):

$$\begin{aligned}
\hat{F}_m^m(\xi,\tilde{z}) &= A_m(\xi)\exp(-\lambda_1\tilde{z}) + B_m(\xi)\exp(-\lambda_2\tilde{z}) \\
&+ C_m(\xi)\exp(-\lambda_3\tilde{z}) \\
&+ D_m(\xi)\exp(\lambda_1\tilde{z}) + E_m(\xi)\exp(\lambda_2\tilde{z}) + G_m(\xi)\exp(\lambda_3\tilde{z}), \\
\hat{\chi}_m^m(\xi,\tilde{z}) &= H_m(\xi)\exp(-\lambda_4\tilde{z}) + K_m(\xi)\exp(\lambda_4\tilde{z})
\end{aligned} \tag{26}$$

It is clear that in a semiinfinite space there is no reflected wave from infinity. When the half-space is truncated by considering a PML around the near field, the wave will not reflect from the far boundary of PML if the amplitudes of outgoing waves attenuate enough through the PML.

The problem is completely solved if eight unknown coefficient functions of the potential functions 26 which are related to the forward wave propagation and their reflection from the far boundary of PML, are obtained via the boundary conditions 13 and 15. One can rewrite the boundary conditions 17 and 18 as 27 in order to the solutions are simply inverted from the Hankel transformed space

$$\begin{aligned}
\nu_{1m} &= \frac{1}{2}\left[\left(\hat{u}_{rm}^{m+1} + i\hat{u}_{\theta m}^{m+1}\right) - \left(\hat{u}_{rm}^{m-1} - i\hat{u}_{\theta m}^{m-1}\right)\right], \nu_{2m} = \hat{u}_{zm}^m \\
\nu_{3m} &= \frac{1}{2}\left[\left(\hat{u}_{rm}^{m+1} + i\hat{u}_{\theta m}^{m+1}\right) + \left(\hat{u}_{rm}^{m-1} - i\hat{u}_{\theta m}^{m-1}\right)\right], \nu_{4m} = \hat{p}_m^m \\
\tau_{1m} &= \frac{1}{2}\left[\left(\hat{\sigma}_{zrm}^{m+1} + i\hat{\sigma}_{z\theta m}^{m+1}\right) - \left(\hat{\sigma}_{zrm}^{m-1} - i\hat{\sigma}_{z\theta m}^{m-1}\right)\right], \tau_{2m} = \hat{\sigma}_{zzm}^m \\
\tau_{3m} &= \frac{1}{2}\left[\left(\hat{\sigma}_{zrm}^{m+1} + i\hat{\sigma}_{z\theta m}^{m+1}\right) + \left(\hat{\sigma}_{zrm}^{m-1} - i\hat{\sigma}_{z\theta m}^{m-1}\right)\right], \tau_{4m} = \hat{q}_{zm}^m
\end{aligned} \tag{27}$$

Note that, in this problem, υ_{jm} $(j = 1$ to $4)$, are related to the conditions at the boundary of PML $\tilde{z}(z = z_T)$, and τ_{jm} with $j = 1$ to 4 are for the near field boundary condition $\tilde{z}(z = 0)$. By virtue of the boundary conditions 13 and 15, the following system of linear algebraic equations may be established, whose solutions are the unknown functions $A_m(\xi)$ to $K_m(\xi)$:

$$\begin{bmatrix}\nu_{1m}\\ \nu_{2m}\\ \nu_{4m}\\ \tau_{1m}\\ \tau_{2m}\\ \tau_{4m}\end{bmatrix} = \begin{bmatrix} -\Phi_1 & -\Phi_2 & -\Phi_3 & \Phi_1 & \Phi_2 & \Phi_3 \\ \Psi_1 & \Psi_2 & \Psi_3 & \Psi_1 & \Psi_2 & \Psi_3 \\ -\Gamma_1 & -\Gamma_2 & -\Gamma_3 & \Gamma_1 & \Gamma_2 & \Gamma_3 \\ \Omega_1 & \Omega_2 & \Omega_3 & \Omega_1 & \Omega_2 & \Omega_3 \\ -\Lambda_1 & -\Lambda_2 & -\Lambda_3 & \Lambda_1 & \Lambda_2 & \Lambda_3 \\ \Theta_1 & \Theta_2 & \Theta_3 & \Theta_1 & \Theta_2 & \Theta_3 \end{bmatrix}\begin{bmatrix} A_m(\xi)e^{-\lambda_1\tilde{z}} \\ B_m(\xi)e^{-\lambda_2\tilde{z}} \\ C_m(\xi)e^{-\lambda_3\tilde{z}} \\ D_m(\xi)e^{\lambda_1\tilde{z}} \\ E_m(\xi)e^{\lambda_2\tilde{z}} \\ G_m(\xi)e^{\lambda_3\tilde{z}} \end{bmatrix} \tag{28}$$

and

$$\begin{bmatrix}\nu_{3m}\\ \tau_{3m}\end{bmatrix} = \begin{bmatrix} -i\xi & -i\xi \\ i\xi C_{1313}\lambda_4 & -i\xi C_{1313}\lambda_4 \end{bmatrix}\begin{bmatrix} H_m(\xi)e^{-\lambda_4\tilde{z}} \\ K_m(\xi)e^{\lambda_4\tilde{z}} \end{bmatrix} \tag{29}$$

where

$$\begin{aligned}
\Phi_i(\xi) &= \bar{k}_1\beta_3\xi\lambda_i\left[\hat{\square}_{pm,i}^2 - \frac{\bar{\alpha}_1\bar{k}_3}{\beta_3\bar{k}_1}\left(\rho_f\omega^2 + \eta\frac{\bar{\alpha}_3}{\bar{k}_3}i\omega\right)\right] \\
\Psi_i(\xi) &= \bar{k}_1\left[\left(\hat{\square}_{0m,i}^2 - \beta_1\xi^2\right)\hat{\square}_{pm,i}^2 + \bar{\alpha}_1\xi^2\left(\rho_f\omega^2 + \eta\frac{\bar{\alpha}_1}{\bar{k}_1}i\omega\right)\right] \\
\Gamma_i(\xi) &= \lambda_i\left[\bar{\alpha}_3\eta i\omega\left(\hat{\square}_{0m,i}^2 - \left(\beta_1 - \beta_3\frac{\bar{\alpha}_1}{\bar{\alpha}_3}\right)\xi^2\right)\right. \\
&\quad \left. + \bar{k}_3\rho_f\omega^2\left(\hat{\square}_{0m,i}^2 - \left(\beta_1 - \beta_3\frac{\bar{k}_1}{\bar{k}_3}\right)\xi^2\right)\right] \\
\Omega_i(\xi) &= -C_{1313}\bar{k}_1\xi\left(\hat{\square}_{cm,i}^2 - \beta_3\lambda_i^2\hat{\square}_{am,i}^2\right) \\
\Lambda_i(\xi) &= C_{1133}\bar{k}_1\beta_3\xi^2\lambda_i\hat{\square}_{am,i}^2 + C_{3333}\bar{k}_1\lambda_i\hat{\square}_{cm,i}^2 \\
\Theta_i(\xi) &= \frac{\bar{k}_3}{\eta}(-\lambda_i\Gamma_i(\xi) + \rho_f\omega^2\Psi_i(\xi)) \\
\hat{\square}_{pm,i}^2 &= \frac{1}{s_k^2}\lambda_i^2 - \xi^2 - i\omega\beta_k \\
\hat{\square}_{0m,i}^2 &= \beta_2\lambda_i^2 - \xi^2 + \bar{\rho}\omega^2 \\
\hat{\square}_{am,i}^2 &= \hat{\square}_{pm,i}^2 - \frac{\bar{\alpha}_1\bar{k}_3}{\beta_3\bar{k}_1}\left(\rho\omega^2 + i\omega\eta\frac{\bar{\alpha}_3}{\bar{k}_3}\right) \\
\hat{\square}_{cm,i}^2 &= \left(\hat{\square}_{0m,i}^2 - \beta_1\xi^2\right)\hat{\square}_{pm,i}^2 + \bar{\alpha}_1\xi^2\left(\rho_f\omega^2 + i\omega\eta\frac{\bar{\alpha}_1}{\bar{k}_1}\right)
\end{aligned} \tag{30}$$

Substituting the solution of Equations (28) into Equations (20) and doing some algebraic manipulations, results in the displacements, pore fluid pressure and stresses in the Hankel–Fourier transformed space. Then, applying the theorem of inverse Hankel integral transforms to these functions, the Fourier components of the displacements, pore fluid pressure and the stresses are obtained as follows:

$$
\begin{aligned}
u_{\tilde{r}} &= \frac{1}{2}\sum_{m=-1}^{1}\exp(im\theta)\left\{\int_0^\infty \xi[(\nu_{3m}-\nu_{1m})J_{m-1}(\tilde{r}\xi)\right.\\
&\left.+(\nu_{3m}+\nu_{1m})J_{m+1}(\tilde{r}\xi)]d\xi\right\}\\
u_{\tilde{\theta}} &= \frac{i}{2}\sum_{m=-1}^{1}\exp(im\theta)\{\int_0^\infty \xi[(\nu_{3m}-\nu_{1m})J_{m-1}(\tilde{r}\xi)\\
&-(\nu_{3m}+\nu_{1m})J_{m+1}(\tilde{r}\xi)]d\xi\}\\
u_{\tilde{z}} &= \sum_{m=-1}^{1}\exp(im\theta)\left\{\int_0^\infty \xi\nu_{2m}J_m(\tilde{r}\xi)d\xi\right\}\\
p &= \sum_{m=-1}^{1}\exp(im\theta)\left\{\int_0^\infty \xi\nu_{4m}J_m(\tilde{r}\xi)d\xi\right\}\\
\sigma_{\tilde{r}\tilde{z}} &= \frac{1}{2}\sum_{m=-1}^{1}\exp(im\theta)\left\{\int_0^\infty \xi[(\tau_{3m}-\tau_{1m})J_{m-1}(\tilde{r}\xi)\right.\\
&\left.+(\tau_{3m}+\tau_{1m})J_{m+1}(\tilde{r}\xi)]d\xi\right\}\\
\sigma_{\tilde{\theta}\tilde{z}} &= \frac{i}{2}\sum_{m=-1}^{1}\exp(im\theta)\left\{\int_0^\infty \xi[(\tau_{3m}-\tau_{1m})J_{m-1}(\tilde{r}\xi)\right.\\
&\left.+(\tau_{3m}+\tau_{1m})J_{m+1}(\tilde{r}\xi)]d\xi\right\}\\
\sigma_{\tilde{z}\tilde{z}} &= \sum_{m=-1}^{1}\exp(im\theta)\left\{\int_0^\infty \xi\tau_{2m}J_m(\tilde{r}\xi)d\xi\right\}\\
q_{\tilde{z}} &= \sum_{m=-1}^{1}\exp(im\theta)\left\{\int_0^\infty \xi\tau_{4m}J_m(\tilde{r}\xi)d\xi\right\}
\end{aligned}
\tag{31}
$$

3.3 | Family of Stretched Coordinate System

As it can be seen from Equations (31), the displacements and pore fluid pressure due to the patch load consist of some exponential functions $\exp(-\lambda_j\tilde{z})$ and Bessel functions $J_m(\tilde{r}\xi)$. The stretched coordinate system should be chosen in such a way that the coordinates remain unchanged in the near field, i.e., $\tilde{z}=z$ and $\tilde{r}=r$, and forcing the outgoing waves to be attenuated in PML. One should notice that θ varies in a finite interval, meaning that no attenuation needs to be considered in terms of θ. Thus, $\tilde{\theta}$ is considered to be equal to θ everywhere. Based on these reasons, the stretching functions are proposed to be in the form of

$$
\begin{aligned}
&\lambda_r(r)=1+f_r(r)H(r-r_N), \qquad \lambda_\theta(\theta)=1,\\
&\lambda_z(z)=1+f_{1z}(z)H(z-z_N)-if_{2z}(z)H(z-z_N)
\end{aligned}
\tag{32}
$$

in which, r_N and z_N represent the radius and depth of open cylindrical region that define the near field and H is the unit-step (Heaviside step) function. The functions $f_r(r)$, $f_{1z}(z)$, and $f_{2z}(z)$, in 32, are selected in such a way that their definite integration in any interval from $b\geq 0$ to $c>b$ to be positive. $F_r(r)$, $F_{1z}(z)$, and $F_{2z}(z)$ are defined as the finite integration of $f_r(r)$, $f_{1z}(z)$, and $f_{2z}(z)$ in the form of

$$
F_r(r)=\int_0^r f_r(s)ds, \qquad F_{jz}(z)=\int_0^z f_{jz}(s)ds, \quad j=1,2 \tag{33}
$$

Thus, the functions $F_r(r)$, $F_{1z}(z)$, and $F_{2z}(z)$ are always positive.

To investigate the forms for the functions $F_{1z}(z)$ and $F_{2z}(z)$, first the complex valued function λ_j is written in terms of its real and imaginary parts in a Cartesian complex coordinate system as $\lambda_j=\gamma_j+i\kappa_j$, with the properties of $\gamma_j>0$ and $\kappa_j>0$. Then, with the use of Equation (32), the exponential function $\exp(-\lambda_j\tilde{z})$ can be written as

$$
\begin{aligned}
\exp(-\lambda_j\tilde{z}) &= \exp(-(\gamma_j+i\kappa_j)(z+F_{1z}(z)-iF_{2z}(z)))\\
&=\exp(-(\gamma_j+i\kappa_j)z)\exp(-\gamma_jF_{1z}(z)\\
&\quad -\kappa_jF_{2z}(z))\exp(-i(\kappa_jF_{1z}(z)-\gamma_jF_{2z}(z)))
\end{aligned}
\tag{34}
$$

Clearly, the exponential function is attenuated by $\exp(-\gamma_jF_{1z}(z)-\kappa_jF_{2z}(z))$; the larger the values of γ_j and κ_j, the faster the exponential function attenuates. Accordingly, the following families of functions for $f_{1z}(z)$ and $f_{2z}(z)$ are employed:

$$
f_{jz}(z)=\beta_{jz}\frac{(z-z_N)^{m_j}}{z_P^{m_j}}, \qquad j=1,2 \tag{35}
$$

in which z_P is the depth of PML along z-direction, β_{jz} and m_j are parameters to be used to speed up/down the attenuation. It is clear that the functions $f_{1z}(z)$ and $f_{2z}(z)$ are defined for $z>z_N$. In this way, one may introduce a family of complex valued coordinate stretching functions in the z-direction as

$$
\lambda_z(z)=1+\beta_{jz}\frac{(z-z_N)^{m_j}}{z_P^{m_j}}H(z-z_N) \tag{36}
$$

It may be recognized that the larger the values of $\beta_{jz}>0$, the faster the exponential function attenuates. It should be mentioned that the function F_{jz} at $\tilde{z}=z_N+z_P$ is given by $F_{jz}(z_N+z_P)=\beta_{jz}z_P/(m_j+1)$. Thus, the wave amplitude at the far boundary of PML, where $\tilde{z}=z_N+z_P$, increases by choosing the larger values for m_j and the accuracy of the results then decreases. Note that, to guarantee the positivity of $F_{jz}(z)$, m_j should be larger than -1. On the other hand, the larger values for z_P improves the accuracy of the results. It is also worth mentioning that the stretching function λ_z at $z=z_N$ equals unity, which means that the z–coordinate is not stretched at the interface of the near field and far field, while the larger the distance from this interface, the larger the stretched coordinate happens in the far field. In the same way, the function $f_r(r)$ and the coordinate stretching functions in the r-direction are considered as

$$
f_r(r)=(r-r_N)\exp(\beta_r(r-r_N)) \tag{37}
$$

and

$$
\lambda_r(r)=1+(r-r_N)\exp(\beta_r(r-r_N))H(r-r_N) \tag{38}
$$

respectively. In fact, substituting the function 38 in the argument of the Bessel function results in

$$J_m(\tilde{r}) = J_m(1 + F_r(r)\mathrm{H}(r - r_N)) = J_m(r + \int_0^r f_r(r)\mathrm{H}(r - r_N)ds)$$
$$= J_m\left(r + \left[\left(\frac{r - r_N}{\beta_r} - \frac{1}{\beta_r{}^2}\right)\exp(\beta_r(r - r_N)) + \frac{1}{\beta_r{}^2}\right]\mathrm{H}(r - r_N)\right) \tag{39}$$

which makes the Bessel function, due to existing of exponential function with $\beta_r > 0$, to be evaluated at points very far from the origin compared with the physical coordinate r, meaning that the larger the value of β_r leads to the response functions approach zero as fast as the Bessel function does. Eventually, substituting 37 and 38 into 8 yields the stretched coordinates in $z-$ and r-directions as

$$\tilde{z} = z + \beta_{1z}\frac{(z - z_N)^{m_1+1}}{(m_1 + 1)z_P^{m_1}}H(z - z_N) - i\beta_{2z}\frac{(z - z_N)^{m_2+1}}{(m_2 + 1)z_P^{m_2}}H(z - z_N)$$
$$\tilde{r} = r + \left[\left(\frac{r - r_N}{\beta_r} - \frac{1}{\beta_r{}^2}\right)\exp(\beta_r(r - r_N)) + \frac{1}{\beta_r{}^2}\right]H(r - r_N) \tag{40}$$

respectively. It is worth mentioning that, in comparison with the physical coordinate system, using stretched coordinates (40) in the kernel of the Hankel transform, which is the Bessel function, causes faster attenuation of the integrands of Equation (31). Thus, the proposed stretched coordinates can enhance the computational efficiency and reduce the time cost.

4 | Degenerated Cases

In this section, some useful degenerations of the general formulation are investigated.

4.1 | Torsion-Less Axisymmetric Problems

In this section, the degeneration of the previously given formulations for the case of torsion-less axis- symmetric is presented. This case happens if the external time-harmonic load is vertical and independent of θ, and the patch of the load is itself axis-symmetric. Under these conditions, the nonzero components of the external excitation, which are independent of the coordinate $\tilde{\theta} = \theta$, are given as

$$P = Q = 0, \; R(\tilde{r}, \tilde{\theta}, t) = R(\tilde{r})\exp(i\omega t), \qquad (\tilde{r}, \tilde{\theta}) \in \pi_0 \tag{41}$$

and its Fourier series contain only one term related to $m = 0$, which is equal to $R(\tilde{r})\exp(i\omega t)$:

$$R_0(\tilde{r}) = R(\tilde{r}) \tag{42}$$

Due to the symmetry of both excitation and geometry, the Fourier series of the solutions also contain only one term related to $m = 0$, and that term equals the solution itself. In this case all boundary conditions are equal to zero except $\tau_{2m} = -J_1(\xi a)/\pi\xi a$. The displacements, pore fluid pressure and stresses for this case are presented in Appendix A.

4.2 | Half-Space Under Asymmetric Patch Load

A saturated poroelastic half-space is considered to be under a uniform surface horizontal circular patch load of radius a and of magnitude $f_h = \sqrt{P^2 + Q^2}$, in which

$$P(\tilde{r}, \tilde{\theta}, t) = \frac{f_h \cos\tilde{\theta}}{\pi a^2}\exp(i\omega t),$$
$$Q(\tilde{r}, \tilde{\theta}, t) = -\frac{f_h \sin\tilde{\theta}}{\pi a^2}\exp(i\omega t),$$
$$R(\tilde{r}, \tilde{\theta}, t) = 0, \qquad (\tilde{r}, \tilde{\theta}) \in \pi_0 \tag{43}$$

Since, the sum of a vertical axis-symmetric and a horizontal force make an arbitrary load, this case can be considered as a general asymmetric case for the problem in hand. The displacements, pore fluid pressure and stresses for this case are presented in Appendix B.

4.3 | Dry Transversely Isotropic Elastic Material

To degenerate the solution for the problems in transversely isotropic elastic half-space from the solution presented for the wave propagation in poroelastic transversely isotropic half-space, one can set $\rho_f = \eta = \alpha_1 = \alpha_3 = 0$. Then defining $\breve{F} = \bar{k}_1\Box_p^2 F$ (see [8]), Equations (9) and 11 are reduced to

$$u_{\tilde{r}} = -\beta_3\frac{\partial^2\breve{F}}{\partial\tilde{r}\partial\tilde{z}} - \frac{1}{\tilde{r}}\frac{\partial\chi}{\partial\tilde{\theta}}, \qquad u_{\tilde{\theta}} = -\beta_3\frac{1}{\tilde{r}}\frac{\partial^2\breve{F}}{\partial\tilde{\theta}\partial\tilde{z}} - \frac{\partial\chi}{\partial\tilde{\theta}},$$
$$u_{\tilde{z}} = \left(\Box_0^2 + \beta_1\nabla_{\tilde{r}\tilde{\theta}}^2\right)\breve{F} \tag{44}$$

and

$$\beta_2\left[(1 + \beta_1)\left(\Box_1^2\Box_2^2 - \bar{\rho}\delta_3\frac{\partial^2}{\partial t^2}\frac{\partial^2}{\partial\tilde{z}^2}\right)\right]\breve{F} = 0, \qquad \Box_0^2\chi = 0 \tag{45}$$

Transferring Equation (45) into the Hankel–Fourier space results in

$$\left[\Box_{1m}\Box_{2m} - \bar{\rho}\omega^2\frac{d^2}{d\tilde{z}^2}\right]\breve{F}_m^m(\xi, \tilde{z}) = 0, \qquad \Box_{0m}\chi_m^m(\xi, \tilde{z}) = 0 \tag{46}$$

where

$$\Box_{0m} = \bar{\rho}\omega^2 - \xi^2 + \beta_2\frac{d^2}{d\tilde{z}^2}, \qquad \Box_{1m} = \frac{\bar{\rho}\omega^2}{1 + \beta_1} - \xi^2 + \frac{1}{s_1^2}\frac{d^2}{d\tilde{z}^2},$$
$$\Box_{2m} = \frac{\bar{\rho}\omega^2}{\beta_2} - \xi^2 + \frac{1}{s_2^2}\frac{d^2}{d\tilde{z}^2} \tag{47}$$

Because of regularity condition, the displacements and stresses approach zero at infinity, with the same conditions for the potential functions. Thus, the potential functions should be zero at the PML boundary. In this way, the solutions to ODEs 46 can be written in the following form:

$$\breve{F}_m^m(\xi, \tilde{z}) = A_m(\xi)\exp(-\lambda_1\tilde{z}) + B_m(\xi)\exp(-\lambda_2\tilde{z}),$$
$$\chi_m^m(\xi, \tilde{z}) = C_m(\xi)\exp(-\lambda_3\tilde{z}) \tag{48}$$

where

TABLE 1 | Material coefficients of saturated porous transversely isotropic half-space [47].

C_{11} N/mm^2	C_{33} N/mm^2	C_{44} N/mm^2	C_{66} N/mm^2	C_{13} N/mm^2	n %	K_s N/mm^2	K_f N/mm^2	ρ_s Kg/m^3	ρ_f Kg/m^3	k_1 m^2	k_3 m^2	η PaS
9570	8320	3000	4190	2330	20	35,000	2250	2600	1000	10^{-12}	10^{-13}	10^{-3}

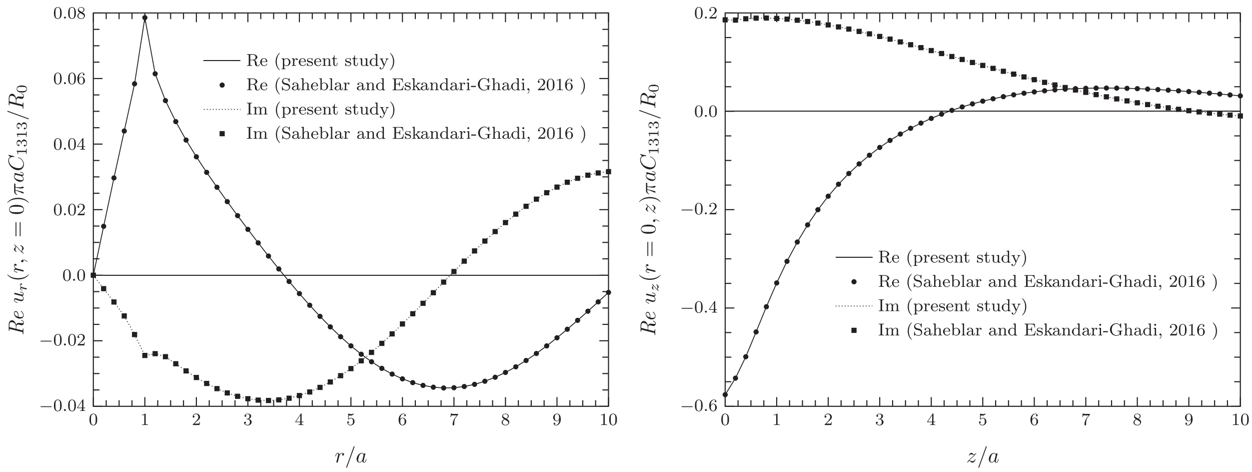

FIGURE 2 | Comparison of the displacements in the physical and stretched coordinate systems for the axisymmetric problem. In the case $\lambda_r = \lambda_z = 1$, the response functions in the stretched coordinate system are not attenuated.

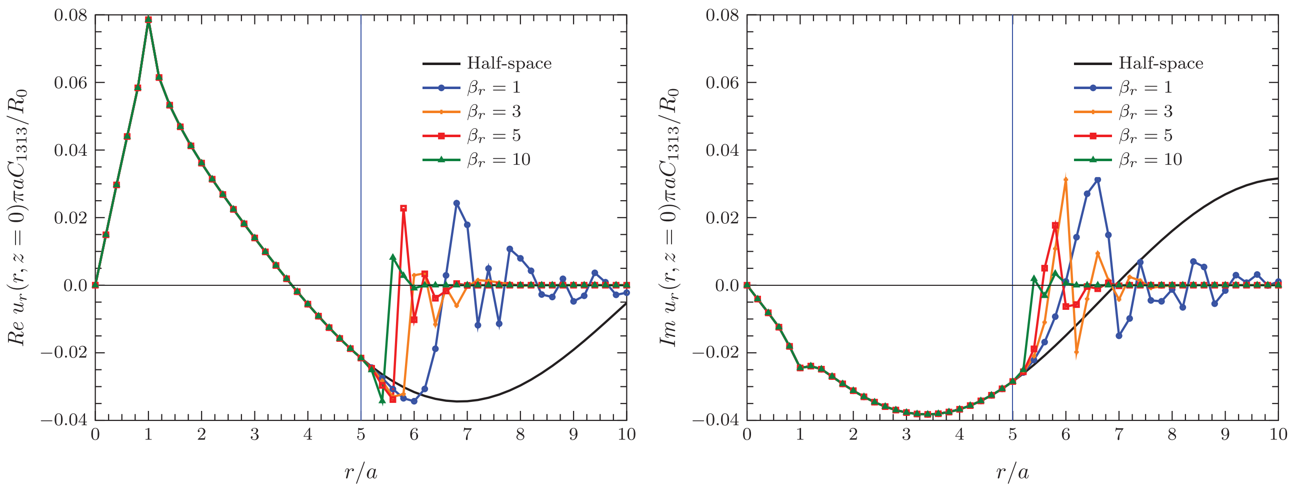

FIGURE 3 | The effect of parameter β_r on the attenuation of functions along the r-axis. The power of amplitude attenuation is directly related to β_r.

$$\lambda_1 = \sqrt{a_1\xi^2 + a_2 + \frac{1}{2}\sqrt{a_3\xi^4 + a_4\xi^2 + a_5}},$$

$$\lambda_2 = \sqrt{a_1\xi^2 + a_2 - \frac{1}{2}\sqrt{a_3\xi^4 + a_4\xi^2 + a_5}},\ \lambda_3 = \sqrt{\frac{\xi^2 - \bar{\rho}\omega^2}{\beta_2}} \tag{49}$$

$$a_1 = \frac{1}{2}\left(s_1^2 + s_2^2\right)^2,\ a_2 = \frac{1}{2}\left(\frac{C_{66}}{C_{33}} + \frac{C_{66}}{C_{44}}\right),\ a_3 = \frac{1}{2}\left(s_1^2 - s_2^2\right)^2,$$

$$a_4 = -2\bar{\rho}\omega^2\left[\left(\frac{C_{1212}}{C_{33}} + \frac{C_{1212}}{C_{44}}\right)\left(s_1^2 + s_2^2\right) - 2\frac{C_{11}}{C_{33}}\left(\frac{C_{66}}{C_{11}} + \frac{C_{66}}{C_{44}}\right)\right],$$

$$a_5 = \bar{\rho}^2\omega^4\left(\frac{C_{66}}{C_{33}} - \frac{C_{66}}{C_{44}}\right)^2 \tag{50}$$

The process of solving the elastic problem for every arbitrary boundary condition is straightforward.

5 | Numerical Results

Some numerical results are presented for the proposed formulations to assess the present appropriate values for the attenuation parameters, and to examine the validity, accuracy, and the applicability of the formulations. For the first purpose, a homogeneous porous transversely isotropic half-space filled by the material given in Table 1 is considered, where the material properties are borrowed from [47].

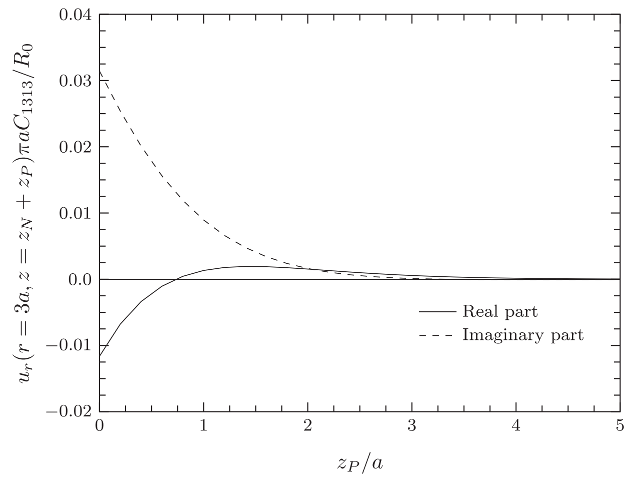

FIGURE 4 | The effect of depth of PML on the attenuation of functions along z-axis. As the PML depth increases the amplitude of response function at the boundary of PML limits to zero. PML, perfectly matched layer.

5.1 | Axisymmetric Problem: Half-Space Under Vertical Patch Load

To verify the formulations and examine their results, the numerical results evaluated in Section 4.1 for a half-space in nonstretched coordinate system are first compared with the analytical results reported in [8]. The displacements for the half-space can be determined by setting $\lambda_r = \lambda_z = 1$. The results for real and imaginary parts of horizontal displacement $u_r(r, z = 0)$ at $z = 0$ in terms of r, and vertical displacement $u_z(r = 0, z)$ at $r = 0$ in terms of z, are compared in Figure 2, where an excellent agreement is observed. Note that a dimensionless frequency of $\omega_0 = \omega a\sqrt{r/C_{44}} = 0.5$ is considered throughout the paper.

Now, a parametric study for attenuation parameters is performed to determine their best range. For this purpose, it should be emphasized that the stretching is applied for r- and z- coordinates. On the other hand, it is noted that the difference between the axis-symmetric and asymmetric is in the order of Bessel functions involved in the expression of the solution. However, different orders of Bessel functions of the first kind behave the same at infinity. Thus, one may study the attenuation parameters for axis-symmetric case and use the results for both the axis-symmetric and asymmetric cases. To this end, first the axis-symmetric vertical surface load is assumed to be applied on a circular patch of radius a with the origin at its center. For this case, the open region defined by $r < 5a$ and $z < 5a$ is considered as the near field, and the lengths of PML along r- and z-direction are considered as $r_P = 5a$ and $z_P = 5a$, respectively. Thus, one may expect exact results for any function in the cylinder defined by $r \leq 5a$ and $z \leq 5a$, and attenuated displacements are desired outside this cylinder.

As recognized from Equations (36) and (38), the higher values for β_{1z}, β_{2z} and β_r may speed up the attenuation of the responses, which means that the higher values for β_{1z}, β_{2z}, and β_r may enhance the accuracy of numerical solution by reducing the amplitude of reflected wave from the far boundary of PML. On the other hand, the higher values of m_1 and m_2 deteriorate the attenuation speed, and therefore cause the accuracy of the results to decrease again due to reflection of the nonzero-amplitude waves from the PML boundary.

To determine proper ranges for the attenuation parameters, a criterion on the values of displacements determined at the PML boundary should be selected. The criterion is defined in such a way that, for example, the displacement at the far boundary PML is less than ϵ times $u_{half-space}$, where $u_{half-space}$ is the value of the same displacement at the same point determined from the solution with $\lambda_r = \lambda_z = 1$. ϵ is a desired small parameter to define the relative error in displacement, and it is selected as 10^{-5} in this study.

Determination of the attenuation parameter along the r-axis is pretty easy, since the attenuation in the r-direction is controlled with only one parameter, say β_r. Figure 3 illustrates the horizontal displacement u_r along the r-direction for different values of β_r. It is observed that the displacement is attenuated very well for $\beta_r > 3$, so, β_r is set to 5 for future illustrations. It should be mentioned that other responses (not shown here) are also attenuated very well.

Before assessing the attenuation parameters in the z-direction, let us investigate the role of the depth of PML z_P. As previously expressed, by increasing the length of PML, where the wave is attenuated through less reflection is expected towards the near field. The dependency of the amplitude of the reflected wave is depicted in Figure 4. It seems that $z_P = 5a$ would be good enough for the rest of computations.

To allocate proper values for the attenuation parameters in the z-direction, first the parameters β_{2z}, m_1, and m_2 are fixed to some arbitrary values, and the parameter β_{1z} is determined. For this purpose, $\beta_{2z} = 5$ and $m_1 = m_2 = 0$ are set. To evaluate the best range for β_{1z}, one may evaluate any response function at a fixed value for r along the z-direction. Figure 5 shows the displacement $u_r(r = 3, z)$ for some values of β_{1z} from zero to 15. It can be inferred that $\beta_{1z} = 10$ can be selected as a proper lower bound. It should be mentioned that, in this case, $u_{r,\mathrm{PML}}(r = 3a, z = 10a)/u_{r,half-space}(r = 3a, z = 10a)$ is less than 10^{-6}. This means that $\beta_{1z} = 10$ may be a good choice for the lower bound of β_{1z}. It should be mentioned that the other responses have the same property.

Based on the same procedure, choosing $\beta_{1z} = 10$ and fixing $m_1 = m_2 = 0$, it can be observed from Figure 6 that the value of 10 may be a proper lower bound for β_{2z}. Eventually, considering $\beta_{1z} = \beta_{2z} = 10$, one can calculate the displacement for different values of m_1 and m_2 (see Figures 7 and 8). However, bearing in mind the restriction of $m_1, m_2 > -1$, and the fact that lower values for these two parameters lead to faster attenuation of displacement results in that $m_1 = m_2 = 0$ would be appropriate values. Consequently, the parameters m_1 and m_2 are eliminated from the stretching function, and by choosing $\beta_{1z} = \beta_{2z} = \beta_z$, the stretching function is transformed to a single parameter (variable) function in the simpler stretched coordinate in the

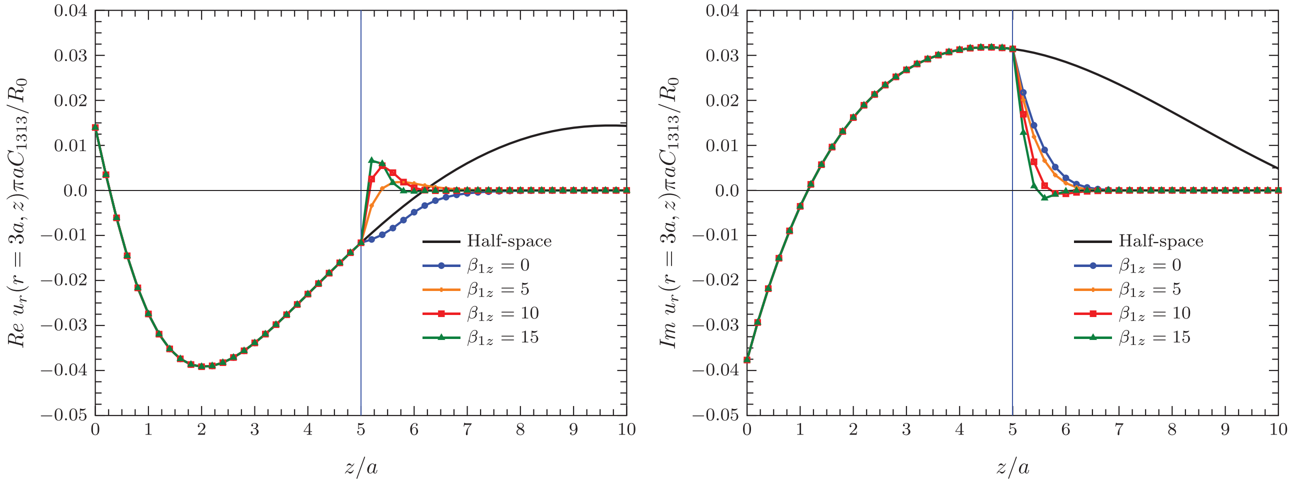

FIGURE 5 | The effect of parameter β_{1z} on the attenuation of functions along the z-axis. The power of amplitude attenuation is directly related to β_{1z}.

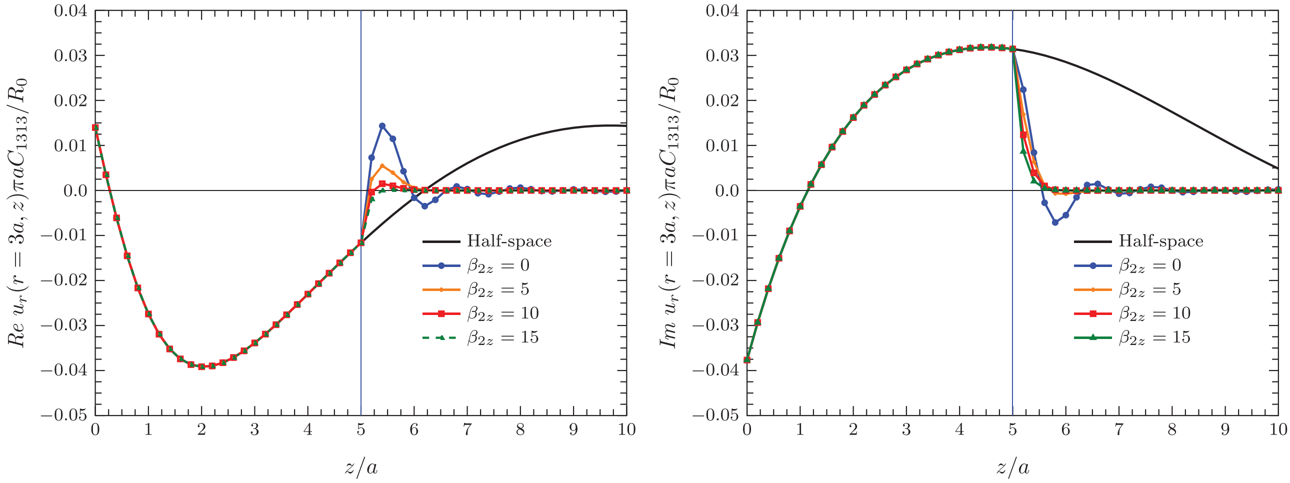

FIGURE 6 | The effect of parameter β_{2z} on the attenuation of functions along the z-axis. The power of amplitude attenuation is directly related to β_{2z}.

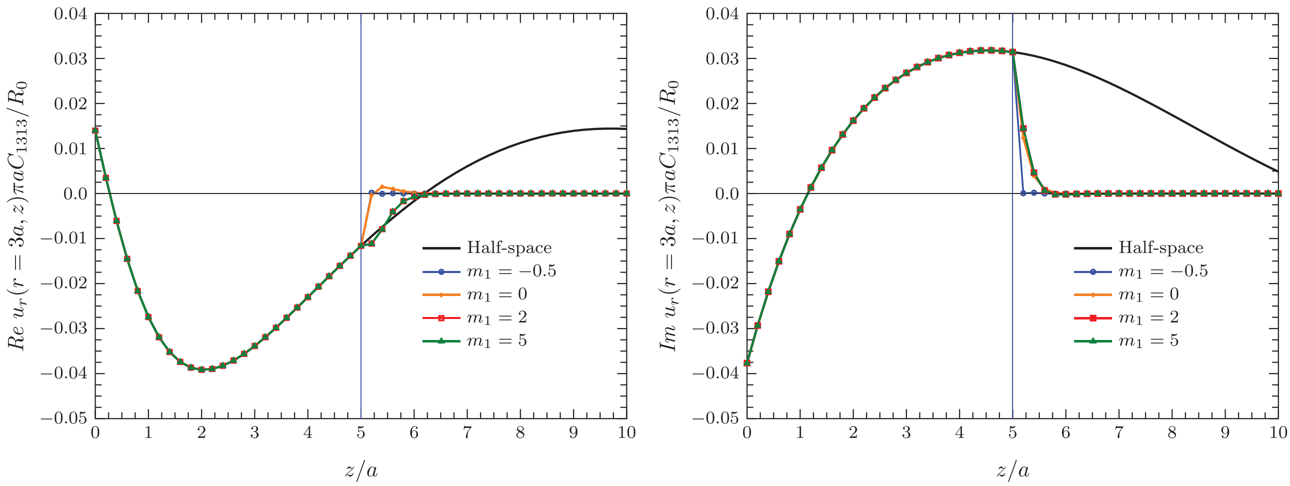

FIGURE 7 | The effect of parameter m_1 on the attenuation of functions along the z-axis. The power of amplitude attenuation is inversely related to m_1.

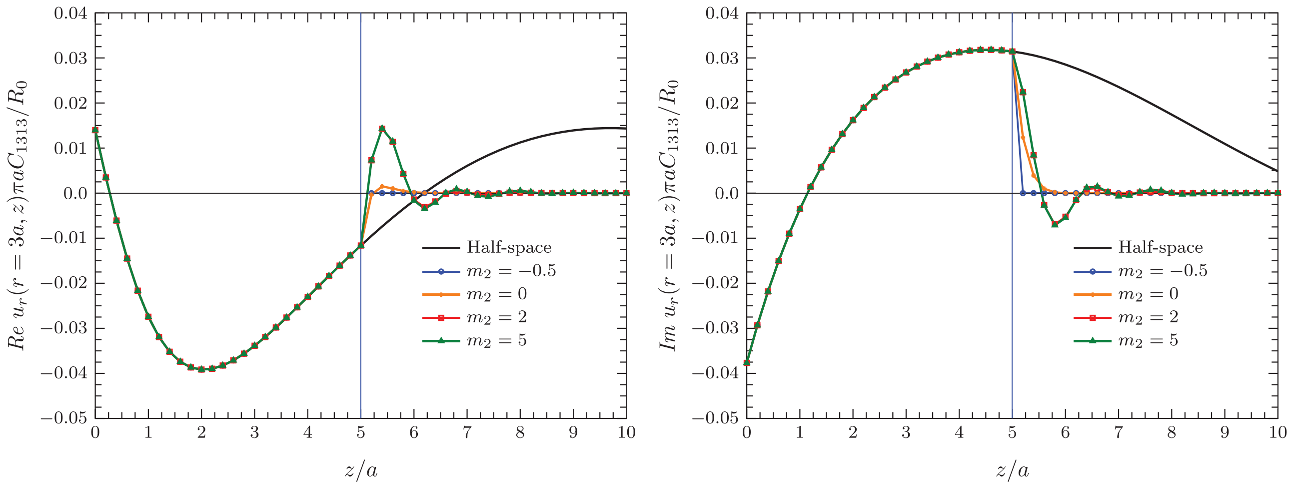

FIGURE 8 | The effect of parameter m_2 on the attenuation of functions along the z-axis. The power of amplitude attenuation is inversely related to m_2.

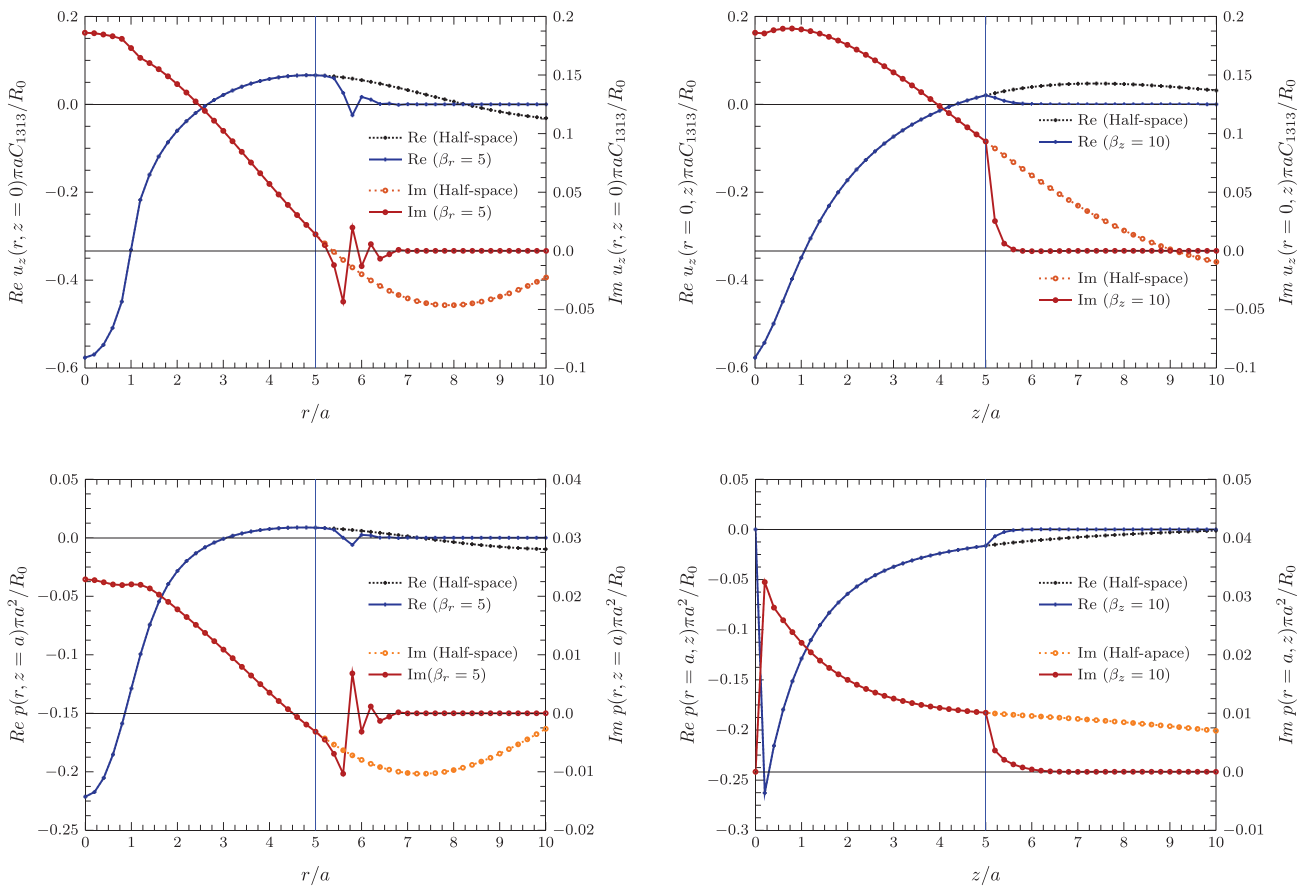

FIGURE 9 | The displacements and pore-pressure for the axisymmetric problem. In each graph, the left and right vertical axes are respectively for the real and imaginary parts of the function and the horizontal axis is common to them.

z-direction. The final expression for the stretched coordinate in z- and r-directions may be written as

$$\tilde{z} = z + (1 - i)\beta_z(z - z_N)H(z - z_N)$$
$$\tilde{r} = r + \left[\left(\frac{r - r_N}{\beta_r} - \frac{1}{\beta_r^2}\right)\exp(\beta_r(r - r_N)) + \frac{1}{\beta_r^2}\right]H(r - r_N) \tag{51}$$

which are determined based on the criterion of

$$u_{\mathrm{PML}}(z_N + z_P)/u_{Half-space}(z_N + z_P) < 10^{-5} \tag{52}$$

In the following, calculation of u_z and p is proceeded based on $\beta_r = 5$ and $\beta_z = 10$. The results are depicted in Figure 9. Also, the ratios of the attenuated amplitudes and the half-space amplitudes are presented in Table 2 which confirm good agreement with the

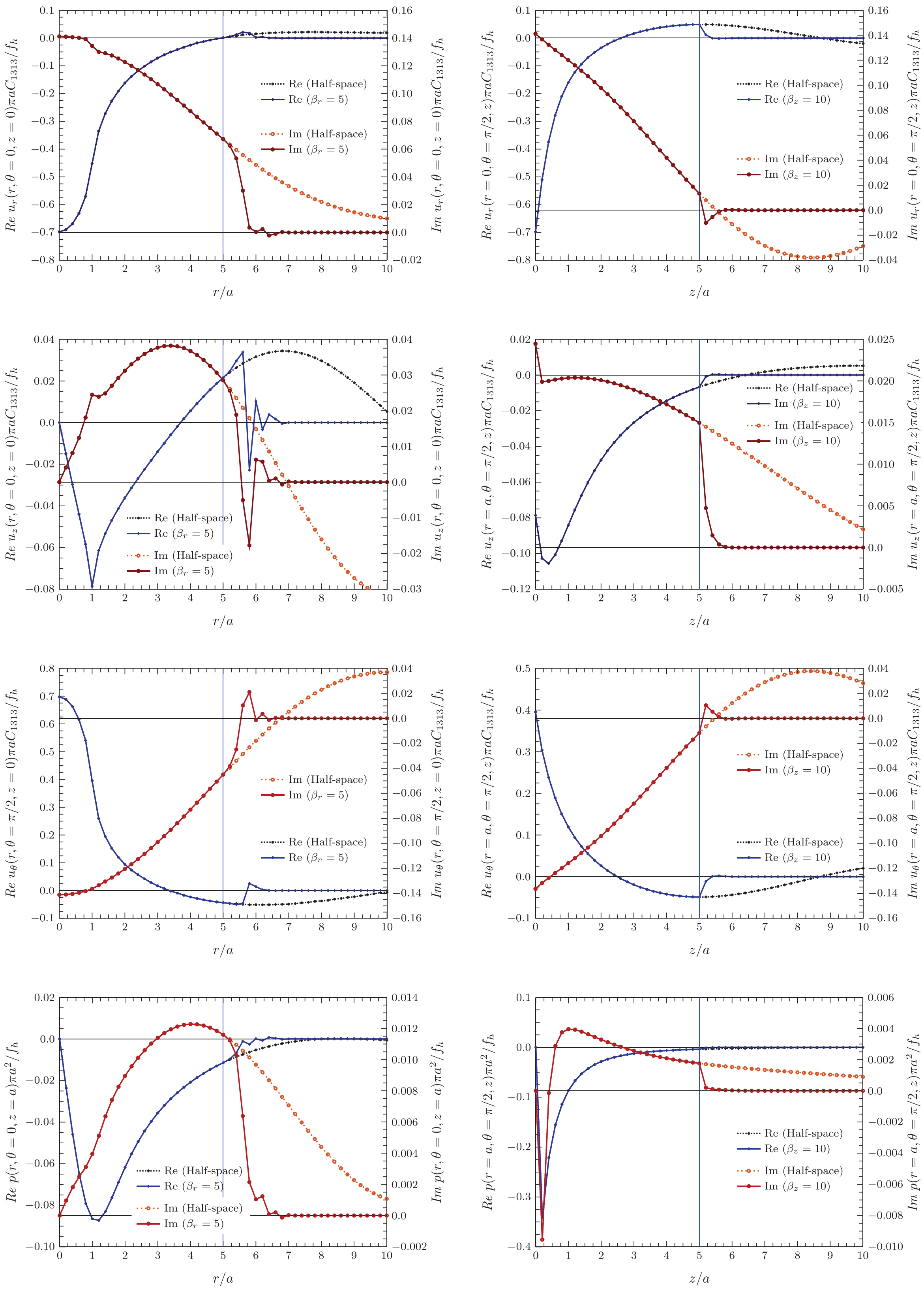

FIGURE 10 | Variations of the displacements and pore-pressure for the half-space under the asymmetric patch load. In each graph, the left and right vertical axes are respectively for the real and imaginary parts of the function and the horizontal axis is common to them.

TABLE 2 | The ratio of the attenuated amplitudes and the half-space amplitudes ($\beta_z = 10$).

Displacements ratio	Real part	Imaginary part
$u_{r,\mathrm{PML}}(r = 3a, z = 10a)/u_{r,half-space}(r = 3a, z = 10a)$	-5.2×10^{-8}	-10^{-7}
$u_{z,\mathrm{PML}}(r = 0, z = 10a)/u_{z,half-space}(r = 0, z = 10a)$	-7×10^{-7}	-1.7×10^{-7}
$p_{\mathrm{PML}}(r = a, z = 10a)/p_{half-space}(r = a, z = 10a)$	3×10^{-7}	-2×10^{-6}

criterion defined in 52.

5.2 | General Problem: Half-Space Under Asymmetric Patch Load

The solution for the half-space under asymmetric patch load is numerically evaluated for $\beta_r = 5$ and $\beta_z = 10$, as determined in previous section for PML and for $\beta_r = \beta_z = 0$, which is required for the actual half-space. Variations of the displacements and pore pressure, evaluated based on Section 4.2, are depicted in Figure 10. Clearly, both displacements and fluid pore pressure are exactly collapsed on the same functions evaluated for the half-space in the near field, whereas they are quickly attenuated in the far field.

6 | Conclusion

In this paper, the requirements and concepts of PML stretching functions to be used in domain-based numerical approach for infinite/semiinfinite BVPs have been investigated. The following concluding remarks can be made:

- An appropriate family of stretching functions has been proposed for each direction in the cylindrical coordinate system to define a standard Biot's formulation in PML. It is also inherently useful in the Cartesian coordinate system.
- The behavior of response functions along any direction in a plane parallel to the free surface of the half-space is different from of the perpendicular one. The proposed family makes it possible to exponentially attenuate the wave energy within PML in any direction.
- The stretching functions have been derived in the both symmetric and asymmetric problems with poroelastic media. The number of parameters for the stretching function along each axis is reduced to one, which is more appropriate in engineering computations.
- The resulted family of the stretched coordinate system can be used in numerical approaches, such as the meshless methods and the FEMs, to analyze more complicated BVPs.

Author Contributions

Kamal Shaker: investigation, calculation, resources, writing – original draft, visualization, software, validation. **Morteza Eskandari-Ghadi**: conceptualization, methodology, validation, writing – review and editing. **Soheil Mohammadi**: validation, writing – review and editing.

Acknowledgments

The partial support from the University of Tehran through 27840/1/ 09 to Morteza Eskandari-Ghadi during this work is gratefully acknowledged.

Conflicts of Interest

The authors declare no conflicts of interest.

Data Availability Statement

The data that support the findings of this study are available from the corresponding author upon reasonable request.

References

1. M. Eskandari-Ghadi, M. Fallahi, and A. Ardeshir-Behrestaghi, "Forced Vertical Vibration of Rigid Circular Disc on a Transversely Isotropic Half-Space," *Journal of Engineering Mechanics* 136, no. 7 (2010): 913–922, https://doi.org/10.1061/(ASCE)EM.1943-7889.0000114.

2. L. Chen, "Forced Vibration of Surface Foundation on Multi-Layered Half Space," *Structural Engineering and Mechanics* 54, no. 4 (2015): 623–648.

3. Z. Zhang and E. Pan, "Vertical and Torsional Vibrations of an Embedded Rigid Circular Disc in a Transversely Isotropic Multilayered Half-Space," *Engineering Analysis with Boundary Elements* 99 (2019): 157–168, https://doi.org/10.1016/j.enganabound.2018.11.013.

4. J. Fu, J. Liang, and B. Han, "Impedance Functions of Three-Dimensional Rectangular Foundations Embedded in Multi-Layered Half-Space," *Soil Dynamics and Earthquake Engineering* 103 (2017): 118–122, https://doi.org/10.1016/j.soildyn.2017.09.024.

5. J. Fu, J. Liang, and Z. Ba, "Non-Singular Boundary Element Method on Impedances of Three-Dimensional Rectangular Foundations," *Engineering Analysis With Boundary Elements* 99 (2019): 100–110, https://doi.org/10.1016/j.enganabound.2018.11.011.

6. T. Senjuntichai, S. Keawsawasvong, and R. Plangmal, "Vertical Vibrations of Rigid Foundations of Arbitrary Shape in a Multi-Layered Poroelastic Medium," *Computers and Geotechnics* 100 (2018): 121–134, https://doi.org/10.1016/j.compgeo.2018.04.012.

7. S. Keawsawasvong and T. Senjuntichai, "Poroelastodynamic Fundamental Solutions of Transversely Isotropic Half-Plane," *Computers and Geotechnics* 106 (2019): 52–67, https://doi.org/10.1016/j.compgeo.2018.10.012.

8. K. Sahebkar and M. Eskandari-Ghadi, "Time-Harmonic Response of Saturated Porous Transversely Isotropic Half-Space Under Surface Tractions," *Journal of Hydrology* 537 (2016): 61–73, https://doi.org/10.1016/j.jhydrol.2016.02.050.

9. M. Shokrollahi, M. Eskandari-Ghadi, and N. Khaji, "A Unified Approach for Stress Wave Propagation in Transversely Isotropic Elastic and Poroelastic Layered Media," *Soil Dynamics and Earthquake Engineering* 157 (2022): 107152, https://doi.org/10.1016/j.soildyn.2022.107152.

10. S. J. Feng, X. H. Ding, Q. T. Zheng, and Z. L. Chen, "Vertical-Rocking-Horizontal Vibrations of a Rigid Disk Resting on Multi-Layered Soils With Groundwater Level," *Applied Mathematical Modelling* 89 (2021): 1491–1516, https://doi.org/10.1016/j.apm.2020.08.009.

11. X. Li, Z. Zhang, and E. Pan, "Wave-Induced Dynamic Response in a Transversely Isotropic and Multilayered Poroelastic Seabed," *Soil Dynamics and Earthquake Engineering* 139 (2020): 106365, https://doi.org/10.1016/j.soildyn.2020.106365.

12. K. Liu, Z. Zhang, and E. Pan, "Dynamic Response of a Transversely Isotropic and Multilayered Poroelastic Medium Subjected to a Moving Load," *Soil Dynamics and Earthquake Engineering* 155 (2022): 107154, https://doi.org/10.1016/j.soildyn.2022.107154.

13. Z. Zhang and E. Pan, "Vertical Vibration of a Rigid Circular Disc Embedded in a Transversely Isotropic and Layered Poroelastic Half-Space," *Engineering Analysis with Boundary Elements* 118 (2020): 84–95, https://doi.org/10.1016/j.enganabound.2020.05.017.

14. Z. Zhang and E. Pan, "Time-Harmonic Response of Transversely Isotropic and Layered Poroelastic Half-Spaces Under General Buried Loads," *Applied Mathematical Modelling* 80 (2020): 426–453, https://doi.org/10.1016/j.apm.2019.11.035.

15. Z. Zhang and E. Pan, "Coupled Horizontal and Rocking Vibrations of a Rigid Circular Disc on the Surface of a Transversely Isotropic and Layered Poroelastic Half-Space," *Applied Mathematical Modelling* 114 (2023): 270–290, https://doi.org/10.1016/j.apm.2022.10.005.

16. S. Chen, "Vertical Vibration of a Flexible Foundation Resting on Saturated Layered Soil Half-Space," *International Journal of Geomechanics* 9, no. 3 (2009): 113–121, https://doi.org/10.1061/(ASCE)1532-3641(2009)9:3(113).

17. T. Senjuntichai and Y. Sapsathiarn, "Forced Vertical Vibration of Circular Plate in Multilayered Poroelastic Medium," *Journal of Engineering Mechanics* 129, no. 11 (2003): 1330–1341, https://doi.org/10.1061/(ASCE)0733-9399(2003)129:11(1330).

18. S. Keawsawasvong, T. Senjuntichai, R. Plangmal, and W. Kaewjuea, "Rocking Vibrations of Rigid Foundations on Multi-Layered Poroelastic Media," *Marine Georesources & Geotechnology* 38, no. 4 (2020): 480–492, https://doi.org/10.1080/1064119X.2019.1597229.

19. S. Keawsawasvong, C. Thongchom, V. Q. Lai, and L. Z. Mase, "Vertical–Horizontal–Rocking Vibrations of Rigid Foundations of Arbitrary Shape on Poroelastic Layer," *Journal of Vibration Engineering & Technologies* 9, no. 7 (2021): 1447–1461, https://doi.org/10.1007/s42417-021-00307-9.

20. D. Givoli, T. Hagstrom, and I. Patlashenko, "Finite Element Formulation With High-Order Absorbing Boundary Conditions for Time-Dependent Waves," *Computer Methods in Applied Mechanics and Engineering* 195, no. 29–32 (2006): 3666–3690, https://doi.org/10.1016/j.cma.2005.01.021.

21. D. Givoli and S. Vigdergauz, "Artificial Boundary Conditions for 2D Problems in Geophysics," *Computer Methods in Applied Mechanics and Engineering* 110, no. 1–2 (1993): 87–101, https://doi.org/10.1016/0045-7825(93)90021-O.

22. R. L. Higdon, "Absorbing Boundary Conditions for Elastic Waves," *Geophysics* 56, no. 2 (1991): 231–241, https://doi.org/10.1190/1.1443035.

23. R. L. Higdon, "Absorbing Boundary Conditions for Acoustic and Elastic Waves in Stratified Media," *Journal of Computational Physics* 101, no. 2 (1992): 386–418, https://doi.org/10.1016/0021-9991(92)90016-R.

24. J. Lysmer and R. L. Kuhlemeyer, "Finite Dynamic Model for Infinite Media," *Journal of the Engineering Mechanics Division* 95, no. 4 (1969): 859–877, https://doi.org/10.1061/jmcea3.0001144.

25. G. D. Manolis and D. E. Beskos, *Boundary Element Methods in Elastodynamics* (Unwin Hyman, 1988).

26. C. Song, "The Scaled Boundary Finite Element Method in Structural Dynamics," *International Journal for Numerical Methods in Engineering* 77, no. 8 (2009): 1139–1171, https://doi.org/10.1002/nme.2454.

27. J. P. Wolf and M. Schanz, "The Scaled Boundary Finite Element Method," *Computational Mechanics* 33, no. 4 (2004): 326–326.

28. U. Basu and A. K. Chopra, "Perfectly Matched Layers for Time-Harmonic Elastodynamics of Unbounded Domains: Theory and Finite-Element Implementation," *Computer methods in applied mechanics and engineering* 192, no. 11–12 (2003): 1337–1375, https://doi.org/10.1016/S0045-7825(02)00642-4.

29. U. Basu and A. K. Chopra, "Perfectly Matched Layers for Transient Elastodynamics of Unbounded Domains," *International Journal for Numerical Methods in Engineering* 59, no. 8 (2004): 1039–1074, https://doi.org/10.1002/nme.896.

30. J. P. Berenger, "A Perfectly Matched Layer for the Absorption of Electromagnetic Waves," *Journal of Computational Physics* 114, no. 2 (1994): 185–200, https://doi.org/10.1006/jcph.1994.1159.

31. W. C. Chew and W. H. Weedon, "A 3D Perfectly Matched Medium From Modified Maxwell's Equations With Stretched Coordinates," *Microwave and Optical Technology Letters* 7, no. 13 (1994): 599–604, https://doi.org/10.1002/mop.4650071304.

32. W. C. Chew and Q. Liu, "Perfectly Matched Layers for Elastodynamics: A New Absorbing Boundary Condition," *Journal of Computational Acoustics* 4, no. 04 (1996): 341–359, https://doi.org/10.1142/S0218396X96000118.

33. D. Givoli, "High-Order Nonreflecting Boundary Conditions Without High-Order Derivatives," *Journal of Computational Physics* 170, no. 2 (2001): 849–870.

34. D. Givoli, "High-Order Local Non-Reflecting Boundary Conditions: A Review," *Wave Motion* 39, no. 4 (2004): 319–326, https://doi.org/10.1016/j.wavemoti.2003.12.004.

35. F. D. Hastings, J. B. Schneider, and S. L. Broschat, "Application of the Perfectly Matched Layer (PML) Absorbing Boundary Condition to Elastic Wave Propagation," *Journal of the Acoustical Society of America* 100, no. 5 (1996): 3061–3069, https://doi.org/10.1121/1.417118.

36. T. Shimada and K. Hasegawa, "Perfectly Matched Layers in the Cylindrical and Spherical Coordinates for Elastic Waves in Solids," *Japanese Journal of Applied Physics* 49, no. 7S (2010): 07HB08, https://doi.org/10.1143/JJAP.49.07HB08.

37. Y. Q. Zeng and Q. H. Liu, "A Staggered-Grid Finite-Difference Method With Perfectly Matched Layers for Poroelastic Wave Equations," *Journal of the Acoustical Society of America* 109, no. 6 (2001): 2571–2580, https://doi.org/10.1121/1.1369783.

38. S. V. Tsynkov, "Numerical Solution of Problems on Unbounded Domains. A review," *Applied Numerical Mathematics* 27, no. 4 (1998): 465–532, https://doi.org/10.1016/S0168-9274(98)00025-7.

39. D. Givoli, *Numerical Methods for Problems in Infinite Domains* (Elsevier, 2013).

40. K. Shaker, M. Eskandari-Ghadi, and S. Mohammadi, "Meshless Method for Wave Propagation in Poroelastic Transversely Isotropic Half-Space With the Use of Perfectly Matched Layer," *International Journal for Numerical and Analytical Methods in Geomechanics* 48, no. 16 (2024): 3751–3779, https://doi.org/10.1002/nag.3797.

41. O. Zienkiewicz, C. Chang, and P. Bettess, "Drained, Undrained, Consolidating and Dynamic Behaviour Assumptions in Soils," *Geotechnique* 30, no. 4 (1980): 385–395, https://doi.org/10.1680/geot.1980.30.4.385.

42. O. Zienkiewicz and T. Shiomi, "Dynamic Behaviour of Saturated Porous Media; the Generalized Biot Formulation and Its Numerical Solution," *International Journal for Numerical and Analytical Methods in Geomechanics* 8, no. 1 (1984): 71–96, https://doi.org/10.1002/nag.1610080106.

43. M. A. Biot, "Mechanics of Deformation and Acoustic Propagation in Porous Media," *Journal of Applied Physics* 33, no. 4 (1962): 1482–1498, https://doi.org/10.1063/1.1728759.

44. M. A. Biot, "Theory of Propagation of Elastic Waves in a Fluid-Saturated Porous Solid. II. Higher Frequency Range," *Journal of the Acoustical Society of America* 28, no. 2 (1956): 179–191, https://doi.org/10.1121/1.1908241.

45. M. A. Biot, "General Solutions of the Equations of Elasticity and Consolidation for a Porous Material," *Journal of Applied Mechanics* 23 (1956): 91–96, https://doi.org/10.1115/1.4011213.

46. W. Chew, J. Jin, and E. Michielssen, "Complex Coordinate Stretching as a Generalized Absorbing Boundary Condition," *Microwave and Optical Technology Letters* 15, no. 6 (1997): 363–369, https://doi.org/10.1002/(SICI)1098-2760(19970820)15:6⟨363::AID-MOP8⟩3.0.CO;2-C.

47. D. P. Schmitt, "Acoustic Multipole Logging in Transversely Isotropic Poroelastic Formations," *Journal of the Acoustical Society of America* 86, no. 6 (1989): 2397–2421, https://doi.org/10.1121/1.398448.

Appendix A: Torsion-Less Axisymmetric Problems

In this case all boundary conditions are equal to zero except $\tau_{2m} = -J_1(\xi a)/\pi\xi a$. Substituting these values in Equation (28) and solving the equations result in A_0, B_0, C_0, D_0, E_0, and G_0 in terms of τ_{2m}. The other unknown coefficients are zero. Thus, with the use of 31, displacements and pore fluid pressure for this case are obtained as follows:

$$\begin{aligned}
\bar{u}_{\bar{r}} = &\int_0^\infty J_1(\bar{r}\xi)\bar{k}_1\beta_3\xi^2\Big\{-\frac{1}{s_k^2}\left[\lambda_1^3(A_0\exp(-\lambda_1\bar{z}) + D_0\exp(\lambda_1\bar{z})) + \lambda_2^3(B_0\,\exp(-\lambda_2\bar{z}) + E_0\,\exp(\lambda_2\bar{z}))\right.\\
&\left.+\lambda_3^3(C_0\,\exp(-\lambda_3\bar{z}) + G_0\,\exp(\lambda_3\bar{z}))\right] + \left[\left((\xi^2 + i\omega\beta_k) + \frac{\bar{\alpha}_1\bar{k}_3}{\beta_3\bar{k}_1}(\rho_f\omega^2 + \eta\frac{\bar{\alpha}_3}{\bar{k}_3}i\omega\right)\right]\\
&\times[\lambda_1(A_0\exp(-\lambda_1\bar{z}) + D_0\exp(\lambda_1\bar{z})) + \lambda_2(B_0\,\exp(-\lambda_2\bar{z}) + E_0\,\exp(\lambda_2\bar{z})) + \lambda_3(C_0\,\exp(-\lambda_3\bar{z}) + G_0\,\exp(\lambda_3\bar{z}))]\}d\xi, \bar{u}_\theta = 0,\\
\bar{u}_{\bar{z}} = &\int_0^\infty \xi J_0(\bar{r}\xi)\Big\{\bar{k}_3\beta_2(\lambda_1^4(A_0\exp(-\lambda_1\bar{z}) + D_0\exp(\lambda_1\bar{z})) + \lambda_2^4(B_0\,\exp(-\lambda_2\bar{z}) + E_0\,\exp(\lambda_2\bar{z}))\\
&+\lambda_3^4(C_0\,\exp(-\lambda_3\bar{z}) + G_0\,\exp(\lambda_3\bar{z}))) - \left[\bar{k}_1\beta_2(\xi^2 + i\omega\beta_k) + \bar{k}_3(1+\beta_1)\left(\xi^2 - \frac{\bar{\rho}\omega^2}{1+\beta_1}\right)\right]\\
&\times[\lambda_1^2(A_0\exp(-\lambda_1\bar{z}) + D_0\exp(\lambda_1\bar{z})) + \lambda_2^2(B_0\,\exp(-\lambda_2\bar{z}) + E_0\,\exp(\lambda_2\bar{z})) + \lambda_3^2(C_0\,\exp(-\lambda_3\bar{z}) + G_0\,\exp(\lambda_3\bar{z}))]\\
&+\left[\bar{k}_1\,(1+\beta_1)\left(\xi^2 - \frac{\bar{\rho}\omega^2}{1+\beta_1}\right)(\xi^2 + i\omega\beta_k) + \bar{k}_1\bar{\alpha}_1\xi^2\left(\rho_f\omega^2 + \eta\frac{\bar{\alpha}_1}{\bar{k}_1}i\omega\right)\right]\\
&\times[(A_0\exp(-\lambda_1\bar{z}) + D_0\exp(\lambda_1\bar{z})) + (B_0\,\exp(-\lambda_2\bar{z}) + E_0\,\exp(\lambda_2\bar{z})) + (C_0\,\exp(-\lambda_3\bar{z}) + G_0\,\exp(\lambda_3\bar{z}))]\Big\}d\xi,\\
\bar{p} = &\int_0^\infty \xi J_0(\bar{r}\xi)\{-\bar{k}_3\beta_2(\rho_f\omega^2 + \eta\frac{\bar{\alpha}_3}{\bar{k}_3}i\omega)\\
&\times[\lambda_1^3(A_0\exp(-\lambda_1\bar{z}) + D_0\exp(\lambda_1\bar{z})) + \lambda_2^3(B_0\,\exp(-\lambda_2\bar{z}) + E_0\,\exp(\lambda_2\bar{z})) + \lambda_3^3(C_0\,\exp(-\lambda_3\bar{z}) + G_0\,\exp(\lambda_3\bar{z}))]\\
&+\left[\bar{k}_3(1+\beta_1)\left(\xi^2 - \frac{\bar{\rho}\omega^2}{1+\beta_1}\right)(\rho_f\omega^2 + \eta\frac{\bar{\alpha}_3}{\bar{k}_3}i\omega) - \bar{k}_1\beta_3\xi^2\left(\rho_f\omega^2 + \eta\frac{\bar{\alpha}_1}{\bar{k}_1}i\omega\right)\right]\\
&[\lambda_1(A_0\exp(-\lambda_1\bar{z}) + D_0\exp(\lambda_1\bar{z})) + \lambda_2(B_0\,\exp(-\lambda_2\bar{z}) + E_0\,\exp(\lambda_2\bar{z})) + \lambda_3(C_0\,\exp(-\lambda_3\bar{z}) + G_0\,\exp(\lambda_3\bar{z}))]\Big\}d\xi.
\end{aligned} \tag{A1}$$

Appendix B: Half-Space Under Asymmetric Patch Load

In this case, the boundary conditions related to stresses in r- and θ- directions for $m = 1$ and -1 are nonzero, and one can write

$$\tau_{1,1} = \frac{J_1(\xi a)}{2\pi\xi a},\ \tau_{1,-1} = \tau_{3,1} = \tau_{3,-1} = -\tau_{1,1} \tag{B1}$$

The corresponding unknown coefficients are obtained by substituting B1 into 28. Finally, the displacements and fluid pore pressure are obtained from 31 as

$$\begin{aligned}
\bar{u}_r = \cos\theta[&\int_0^\infty (J_2(\bar{r}\xi) - J_0(\bar{r}\xi))\bar{k}_1\beta_3\xi^2\{-\frac{1}{s_k^2}(\lambda_1^3A_1\exp(-\lambda_1 z) + \lambda_2^3B_1\exp(-\lambda_2 z) + \lambda_3^3C_1\exp(-\lambda_3 z))\\
&+\left[(\xi^2 + i\omega\beta_k) + \frac{\bar{\alpha}_1\bar{k}_3}{\beta_3\bar{k}_1}\left(\rho_f\omega^2 + \eta\frac{\bar{\alpha}_3}{\bar{k}_3}i\omega\right)\right](\lambda_1A_1\exp(-\lambda_1 z) + \lambda_2B_1\exp(-\lambda_2 z) + \lambda_3C_1\exp(-\lambda_3 z))\}d\xi\\
&-\int_0^\infty (J_2(\bar{r}\xi) + J_0(\bar{r}\xi))\frac{J_1(\xi a)}{2\pi a\lambda_4C_{1313}}\exp(-\lambda_4 z)d\xi],\\
\bar{u}_\theta = \sin\theta[&\int_0^\infty (J_2(r\xi) + J_0(r\xi))\bar{k}_1\beta_3\xi^2\{-\frac{1}{s_k^2}(\lambda_1^3A_1\exp(-\lambda_1 z) + \lambda_2^3B_1\exp(-\lambda_2 z) + \lambda_3^3C_1\exp(-\lambda_3 z))
\end{aligned}$$

$$+\left[(\xi^2+i\omega\beta_k)+\frac{\bar{\alpha}_1\bar{k}_3}{\beta_3\bar{k}_1}(\rho_f\omega^2+\eta\frac{\bar{\alpha}_3}{\bar{k}_3}i\omega)\right](\lambda_1 A_1\exp(-\lambda_1 z)+\lambda_2 B_1\exp(-\lambda_2 z)+\lambda_3 C_1\exp(-\lambda_3 z))\}d\xi$$

$$-\int_0^\infty (J_2(r\xi)-J_0(r\xi))\frac{J_1(\xi a)}{2\pi a\lambda_4 C_{1313}}\exp(-\lambda_4 z)d\xi],$$

$$\bar{u}_z=2\cos\theta[\int_0^\infty \xi J_1(r\xi)\{\bar{k}_3\beta_2(\lambda_1^4 A_1\exp(-\lambda_1 z)+\lambda_2^4 B_1\exp(-\lambda_2 z)+\lambda_3^4 C_1\exp(-\lambda_3 z))$$

$$-\left[\bar{k}_1\beta_2(\xi^2+i\omega\beta_k)+\bar{k}_3(1+\beta_1)\left(\xi^2-\frac{\bar{\rho}\omega^2}{1+\beta_1}\right)\right](\lambda_1^2 A_1\exp(-\lambda_1 z)+\lambda_2^2 B_1\exp(-\lambda_2 z)+\lambda_3^2 C_1\exp(-\lambda_3 z))$$

$$+\left[\bar{k}_1(1+\beta_1)(\xi^2-\frac{\bar{\rho}\omega^2}{1+\beta_1})(\xi^2+i\omega\beta_k)+\bar{k}_1\bar{\alpha}_1\xi^2\left(\rho_f\omega^2+\eta\frac{\bar{\alpha}_1}{\bar{k}_1}i\omega\right)\right]$$

$$\times(A_1\exp(-\lambda_1 z)+B_1\exp(-\lambda_2 z)+C_1\exp(-\lambda_3 z))\}d\xi],$$

$$\bar{p}=2\cos\theta[\int_0^\infty \xi J_1(r\xi)\{-\bar{k}_3\beta_2(\rho_f\omega^2+\eta\frac{\bar{\alpha}_3}{\bar{k}_3}i\omega)(\lambda_1^3 A_1\exp(-\lambda_1 z)+\lambda_2^3 B_1\exp(-\lambda_2 z)+\lambda_3^3 C_1\exp(-\lambda_3 z))$$

$$+\left[\bar{k}_3(1+\beta_1)(\xi^2-\frac{\bar{\rho}\omega^2}{1+\beta_1})(\rho_f\omega^2+\eta\frac{\bar{\alpha}_3}{\bar{k}_3}i\omega)-\bar{k}_1\beta_3\xi^2\left(\rho_f\omega^2+\eta\frac{\bar{\alpha}_1}{\bar{k}_1}i\omega\right)\right]$$

$$\times(\lambda_1 A_1\exp(-\lambda_1 z)+\lambda_2 B_1\exp(-\lambda_2 z)+\lambda_3 C_1\exp(-\lambda_3 z))\}d\xi]. \tag{B2}$$